12-2010

Discontinuous Galerkin Method for 1D Shallow Water Flow with Water Surface Slope Limiter

Wencong Lai
Clemson University, wlai@clemson.edu

DISCONTINUOUS GALERKIN METHOD FOR 1D SHALLOW WATER FLOW WITH WATER SURFACE SLOPE LIMITER

A Thesis

Presented to

the Graduate School of

Clemson University

In Partial Fulfillment

of the Requirements for the Degree

Master of Science

Civil Engineering

---

by

Wencong Lai

December 2010

Accepted by:

Abdul A. Khan, Committee Chair

Taufiquar R. Khan

Nadarajah Ravichandran

ABSTRACT

A water surface slope limiting scheme is applied to numerically solve the one dimensional shallow water equations with bottom slope source term. The total variation diminishing Runge-Kutta discontinuous Galerkin finite element method with slope limiter schemes based on water surface and water depth are investigated for solving one-dimensional shallow water equations. For each slope limiter, three different Riemann solvers based on HLL, LF, and Roe flux functions are used. The three different solvers with slope limiters based on water surface and water depth are applied to simulate idealized dambreak problem, hydraulic jump, quiescent flow, subcritical flow, supercritical flow, and transcritical flow. The proposed water surface based slope limiter scheme is easy to implement and shows better conservation property compared to the slope limiter based on water depth for the tests. Of the three flux functions, the Roe approximation provides the best results while the LF function proves to be least suitable when used with either slope limiter scheme.

TABLE OF CONTENTS

Page

TITLE PAGE i

ABSTRACT ii

LIST OF TABLES v

LIST OF FIGURES vi

CHAPTER

I. INTRODUCITON 1

II. LITERACTURE REVIEW 4

III. NUMEIRICAL SCHEME 9

Governing equations 9

Property of shallow water equations 10

Discontinuous Galerkin formulation 12

Approximate Riemann solvers 13

Time integration 20

Slope limiter 21

IV. NUMERICAL TESTS 24

Test 1: Idealized dambreak 24

Test 2: Hydraulic jump 26

Test 3: Quiescent water over a bump 28

Test 4: Subcritical flow over a bump 31

Test 5: Transcritical flow over a bump 34

Test 6: Supercritical flow over a bump 37

Test 7: Quiescent water over an irregular bed 40

Test 8: Subcritical flow over an irregular bed 43

Test 9: Transcritical flow over an irregular bed 46

V. SUMMARY 49

REFERENCES 51

LIST OF TABLES

Table Page

4-1 Bed elevation variation with distance 40

LIST OF FIGURES

Figure Page

3-1 Discontinuous finite element discretization....12

3-2 Two-wave configuration....14

4-1 Numerical solution of water surface for ideal dambreak....25

4-2 Numerical solution of flow rate for ideal dambreak....25

4-3 Numerical solution of water surface for hydraulic jump....27

4-4 Numerical solution of flow rate for hydraulic jump.... 27

4-5 Numerical solution of water depth for Test 3 with water depth slope limiter....29

4-6 Numerical solution of flow rate for Test 3 with water depth slope limiter 29

4-7 Numerical solution of water depth for Test 3 with water surface slope limiter....30

4-8 Numerical solution of flow rate for Test 3 with water surface slope limiter....30

4-9 Numerical solution of water depth for Test 4 with water depth slope limiter....32

4-10 Numerical solution of flow rate for Test 4 with water depth slope limiter....32

List of Figures (Continued)

Figure Page

4-11 Numerical solution of water depth for Test 4 with water surface slope limiter 33

4-12 Numerical solution of flow rate for Test 4 with water surface slope limiter 33

4-13 Numerical solution of water depth for Test 5 with water depth slope limiter 35

4-14 Numerical solution of flow rate for Test 5 with water depth slope limiter 35

4-15 Numerical solution of water depth for Test 5 with water surface slope limiter 36

4-16 Numerical solution of flow rate for Test 5 with water surface slope limiter 36

4-17 Numerical solution of water depth for Test 6 with water depth slope limiter 38

4-18 Numerical solution of flow rate for Test 6 with water depth slope limiter 38

4-19 Numerical solution of water depth for Test 6 with water surface slope limiter 39

List of Figures (Continued)

Figure Page

4-20 Numerical solution of flow rate for Test 6 with water surface slope limiter 39

4-21 Numerical solution of water depth for Test 7 with water depth slope limiter 41

4-22 Numerical solution of flow rate for Test 7 with water depth slope limiter 41

4-23 Numerical solution of water depth for Test 7 with water surface slope limiter 42

4-24 Numerical solution of flow rate for Test 7 with water surface slope limiter 42

4-25 Numerical solution of water depth for Test 8 with water depth slope limiter 44

4-26 Numerical solution of flow rate for Test 8 with water depth slope limiter 44

4-27 Numerical solution of water depth for Test 8 with water surface slope limiter 45

4-28 Numerical solution of flow rate for Test 8 with water surface slope limiter 45

List of Figures (Continued)

Figure Page

4-29 Numerical solution of water depth for Test 9 with water depth slope limiter....47

4-30 Numerical solution of flow rate for Test 9 with water depth slope limiter....47

4-31 Numerical solution of water depth for Test 9 with water surface slope limiter....48

4-32 Numerical solution of flow rate for Test 9 with water surface slope limiter....48

CHAPTER ONE

INTRODUCTION

Water is one of the most important natural resources in human history, and open channel hydraulic has always been of great interest to researchers and engineers. The free surface flows that take place in rivers, estuaries and oceans are complex phenomenon. Although great advancement in numerical modeling of open channel hydraulics have been achieved, it is still difficult to completely describe open channel flow physically and mathematically.

Analytical solutions of open channel flow equations are generally not available except for some simplified cases. Thus, the numerical solutions for open channel flows are of great significance to researchers and engineers in order to understand these flows.

Over the past several decades, a large amount of numerical models have been built for the open channel flows based on numerical methods like Finite Difference Method (FDM), Finite Volume Method (FVM), Finite Element Method (FEM), etc. Researchers have always been seeking for better numerical methods to model physical phenomenon like open channel flow. In this study, the numerical method called Discontinuous Galerkin (DG) method, which is also called discontinuous finite element method is used to investigate its capability and performance in solving the one-dimensional shallow water equations.

Discontinuous Galerkin method was proposed for the solution of hyperbolic conservation laws to which the one-dimensional shallow water equations belong. The

discontinuous Galerkin method can be viewed as combination of finite volume method and finite element method, so it preserves the advantages of both schemes, such as shock capturing and higher order accuracy. To apply the discontinuous Galerkin method, the main challenges arise from seeking an accurate numerical flux function for the system of equations and proper treatment of its source term. In this study, several available and widely used numerical flux functions are chosen and their accuracy and effectiveness are evaluated for the solution of one-dimensional shallow water flow equations in a variety of flow conditions. Special attention is paid to their ability to preserve the conservative property, capture shock, and order of accuracy.

Besides the numerical flux term, the improperly treatment of the source term will distort the accuracy of the numerical schemes, such as affect the conservative property of the system and generate unphysical flow. Various treatments have been proposed to model the source term in case of finite difference method and finite volume method. For discontinuous Galerkin method, the water surface slope limiter is proposed here for the treatment of source term. And numerical results for water surface slope limiter and water depth slope limiter are compared.

In the study reported herein, the discontinuous Galerkin method with water surface slope limiter in applied to solve the one-dimensional shallow water flow. Literature review and the advantages of discontinuous Galerkin method are presented in Chapter 2. In Chapter 3, description of discontinuous Galerkin method applied to solve the one-dimensional shallow water equations are presented. In Chapter 4, numerical tests are

presented for different flow conditions in open channel to verify the numerical scheme. A summary of this study is presented in Chapter 5.

CHAPTER TWO

LITERECTURE REVIEW

Open channel flow problems are governed by the Shallow Water Equations (SWE), also known as Saint-Venant equations. Over the past decades, a large amount of numerical schemes have been developed to solve the shallow water equations for various applications. The Finite Difference Method (FDM) and Finite Volume Method (FVM) are the two most widely used methods for shallow water equations and fluid dynamics problems. Wang et al. (2000) used a finite difference TVD scheme to compute dambreak problems. Lin et al. (2003) used finite volume method to solve shallow water equations.

In general, Finite Element Method (FEM) is preferred for complex geometries. However, a traditional finite element method fails to model the convective terms in general fluid dynamics problems. Extra efforts are required to overcome this shortcoming, for example, penalty finite element method (Hughes et al. 1979), split-characteristic finite element method (Zienkiewicz and Ortiz 1995), characteristic-mixed finite element method (Arbogast and Wheeler 1995).

In recent years, the Discontinuous Galerkin (DG) method has been developed to solve systems of hyperbolic equations. The DG method was first introduced by Reed and Hill (1973) for the solution of neutron transport equation, a time independent linear hyperbolic equation. Cockburn and Shu (1989) and Cockburn et al. (1989) further advanced the DG method for conservation laws. They incorporated a Total Variation Diminishing (TVD) explicit Runge-Kutta time integration scheme along with flux

limiters or slope limiters to ensure the TVD properties for discontinuous Galerkin method. The Runge-Kutta Discontinuous Galerkin (RKDG) method can be viewed as a combination of the finite volume method and the finite element method. As a result, the RKDG method keeps advantages of both FVM and FEM. As discontinuous element boundary is used, various upwind schemes used in the FVM may be directly incorporated into the RKDG method to deal with convective dominated problems. Like the FEM, the RKDG method can deal with complex geometry conveniently and can utilize higher order spatial approximation. According to Li (2006), the RKDG method provides additional advantages, for example, RKDG method can easily deal with source term as in FEM. By decoupling the elements through the use of boundary flux, a local formulation is achieved that does not require assembling the global matrix and explicit time schemes can be implemented. In practical applications, where millions of elements may be used, the RKDG method will prove advantageous in terms computing speed and memory demand. The RKDG method is a conservative scheme, which is a suitable choice for physical problems, since most physical properties such as mass and momentum are conserved quantities. As the solution of the DG method is discontinuous, it can be easily adopted for problems involving shocks and discontinuities. In addition, the hp-adaptive algorithm is much easier to apply to the RKDG local formulation.

Schwanenberg and Köngeter (2000) were the first to implement the RKDG method for shallow water equations for applications to practical problems like shocks, dambreak problem, and oblique hydraulic jump. Later, Schwanenberg and Harms (2004) used different cases in transcritical flow to investigate the accuracy and convergence of the

RKDG method. Aizinger and Dawson (2002) and Dawson and Aizinger (2005) applied the RKDG method to two-dimensional and three-dimensional shallow water flows. Kubatko et al. (2006) demonstrated the applicability of hp-adaptive algorithm for the RKDG method.

In the DG method, the elements are decoupled and the accuracy with which the boundary flux is calculated determines the performance of the method. The calculation of boundary flux across discontinuous elements becomes a Generalized Riemann Problem (GRP). Since the exact Riemann solvers are tedious and time-consuming, different approximate Riemann solvers are developed in recent decades, such as HLL flux (Harten et al., 1983), Roe flux (Roe, 1981), Osher's flux (Osher and Solomon, 1982) and weighted average flux (Toro, 1989). Schwanenberg and Harms (2004) used RKDG method with HLL flux to test one and two dimensional dam break problems, while Tassi et al. (2007) incorporated HLLC flux for shallow water flow problems.

As in other numerical schemes, using higher order spatial approximation in the RKDG method results in unphysical spurious oscillation near shocks. The Essentially Non-oscillatory (ENO) scheme (Harten et al., 1987) and the Total Variation Diminishing (TVD) scheme are the two widely used methods to reduce oscillations. The key idea in the ENO scheme is to choose the locally smoothest stencil with nonlinear adaptive procedure at the approximation level. Later, Liu et al. (1994) constructed the Weighted Essentially Non-oscillatory (WENO) in a similar way. The ENO and WENO schemes were originally constructed within the framework of the finite volume method and the

finite difference method. Qiu and Shu (2005) applied the WENO limiters with the discontinuous Galerkin finite element method with a similar procedure.

Schemes that satisfy the Total Variation Diminishing (TVD) criterion are oscillation-free schemes as well. Flux limiters and slope limiters are widely used to achieve the TVD property. The key idea for flux limiter and slope limiter is the same. The flux limiter would be applied directly to the fluxes while slope limiter would be applied on conserved variables or primitive variables. For this reason, slope limiter is preferred since it may better preserve the conservative property and reduce oscillations.

Gottlieb and Shu (1998) showed that a TVD spatial discretization may generate oscillation with a non-TVD Runge-Kutta time discretization. Cockburn and Shu (1989) demonstrated that for piecewise polynomials of r^{th} order, with a $(r+1)^{th}$ order TVD time integration, the results were $(r+1)^{th}$ order accurate. They further proved that the scheme was Total Variation Bounded in the Means (TVBM), which is a modification of the TVD property.

In addition to the difficulty of dealing with the convective term in traditional methods, problems arise when the source term appear. Nujić (1995) proposed a non-oscillatory scheme in which the flux function was discretized in a form compatible with the bottom slope term. Garcia-Navarro and Vázquez-Cendón (2000) discussed the difficulties of correct treatment to the geometrical source terms, and proposed the upwind treatment for the source term. Perthame and Simeoni (2001) developed a kinetic formulation for the treatment of source term due to bottom topography in Saint-Venant equations. Zhou et al. (2001) developed the surface gradient method to treat the source

term in the shallow water equation for the data reconstruction. Ying et al. (2004) devised an upwind conservative scheme with a weighted average water surface gradient approach to deal with source term in one dimensional open channel flows. The weighted factors in the upwind scheme were based on the Courant number. Catella and Petrere Jr. (2008) proposed a predictor-corrector finite volume method to compute one-dimensional open channel flows. The proposed method did not need to solve the Riemann problem at cell interface and artificial viscosity or shock-capturing techniques were not needed to capture discontinuities. A Froude number based criterion was used to overcome the difficulty of handling the source term.

In this study, the Runge-Kutta discontinuous Galerkin method with TVD based water surface slope limiting scheme for the source term is proposed for solving one-dimensional shallow water equations. The TVD based slope limiter scheme is usually applied to the conserved variables of the hyperbolic system to preserve the conservative property of the system. Here, the water surface based slope limiter is applied and the numerical results are compared to the slope limiter based on the water depth. Three different flux functions are investigated for each slope limiter scheme. Two channels with variable bed slopes are used to test the two slope limiter schemes with different flow conditions.

CHAPTER THREE

NUMERICAL SCHEME

This chapter provides the details of the numerical scheme using discontinuous finite element method to model the one-dimensional shallow water equations.

Governing Equations

The governing equations for open channel flows are conservation of mass, momentum and energy. For practical applications, the flow rate and water depth are sufficient to describe the flow characteristics. So the conservation of mass and momentum would be sufficient to describe the flow situation. These two equations are usually referred to as Saint-Venant equations. To model one dimensional open channel flow problems with rectangular cross section, the following assumptions are made:

1. The cross section of channel is rectangular;
2. Bed slope is small;
3. The pressure distribution is hydrostatic;
4. No lateral inflow;
5. Velocity distribution is uniform over channel cross section;
6. The scale of cross section is much less than the channel's length scale;
7. Water density is constant;
8. Head loss in unsteady flow can be model as in steady flow;
9. Dependent variables are continuous and differentiable.

With the assumptions stated above, the governing equations for one-dimensional shallow water flow in rectangular channel are:

$$\frac{\partial h}{\partial t}+\frac{\partial q}{\partial x}=0 \tag{3-1}$$

$$\frac{\partial q}{\partial t}+\frac{\partial (q^2/h+gh^2/2)}{\partial x}=gh(S_0-S_f) \tag{3-2}$$

where h =flow depth, q =unit width flow rate, g =gravitational acceleration, the bed slope is given by

$$S_0=-\frac{\partial z_b}{\partial x} \tag{3-3}$$

and the friction slope for steady flow is given by

$$S_f=\frac{n^2 q|q|}{h^{10/3}} \tag{3-4}$$

where n =Manning's roughness coefficient and z_b =channel bed elevation.

Property of shallow water equations

Governing equations (3-1) and (3-2) can be written in conservation form as follows

$$\frac{\partial \mathbf{U}}{\partial t}+\frac{\partial \mathbf{F}}{\partial x}=\mathbf{S} \tag{3-5}$$

with conserved variable vector and flux vector given by, respectively

$$\mathbf{U}=\begin{bmatrix} h \\ q \end{bmatrix} \tag{3-6}$$

$$\mathbf{F} = \begin{bmatrix} q \\ gh^2/2 + q^2/h \end{bmatrix} \tag{3-7}$$

and the source vector and the Jacobian matrix (also called advection matrix) are, respectively, given by

$$\mathbf{S} = \begin{bmatrix} 0 \\ gh(S_0 - S_f) \end{bmatrix} \tag{3-8}$$

$$\mathbf{A} = \frac{\partial \mathbf{F}}{\partial \mathbf{U}} = \begin{bmatrix} 0 & 1 \\ gh - q^2/h^2 & 2q/h \end{bmatrix} \tag{3-9}$$

Eigenvalues of the Jacobian matrix are given by

$$\lambda_{1,2} = q/h \pm \sqrt{gh} = u \pm c \tag{3-10}$$

The eigenvalues given above are real and distinct for both subcritical and supercritical flow ($h \neq 0$). Thus, the governing equations given by (3-5) are hyperbolic partial differential equations (PDE). For hyperbolic PDEs, even with smooth initial conditions and boundary conditions, discontinuous solution may evolve during wave propagation. So numerical model for the shallow water equations should be able to capture these discontinuities, as comparison and discussion above of several numerical methods, the discontinuous finite element method would be an appropriate choice for such problem.

Discontinuous Galerkin Formulation

The one dimensional domain $(x=[0,L])$ is divided into N elements, let $0=x_1<x_2\cdots<x_{N+1}=L$ be a partition of the domain. If $I_i=[x_i,x_{i+1}]$, $1\le i\le N$, a discontinuous piecewise finite element space of polynomials m can be denoted as

$$V^m=\{v:v\,|\,I_i\in P^m(I_i),\ 1\le i\le N\} \tag{3-11}$$

A typical discontinuous element discretization is illustrated in Figure 3-1.

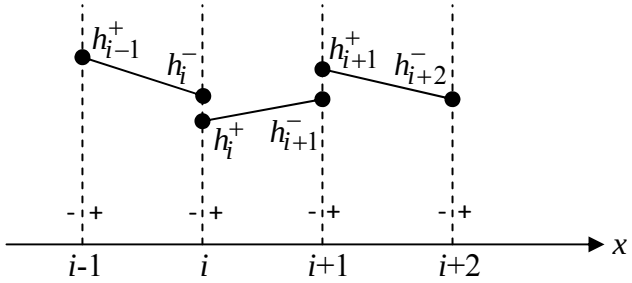

Figure 3-1. Discontinuous finite element discretization

For the sake of simplicity, only linear interpolation is used here to show the discontinuous Galerkin formulation. It may not be the case in application, higher order and even different order elements can be used in spatial discretization.

Inside an element, unknowns are approximated by Lagrange interpolation as follows

$$\hat{\mathbf{U}}=\sum_{j=1}^{2}N_j(x)\mathbf{U}_j \tag{3-12}$$

$$\hat{\mathbf{F}}=\mathbf{F}(\hat{\mathbf{U}}) \tag{3-13}$$

Integrating (3-5) with (3-12) and (3-13) for variable and flux vector, respectively, and using weighting function $W=W(x)$ within an element gives

$$\int_{x_i}^{x_{i+1}} W\left(\frac{\partial \hat{\mathbf{U}}}{\partial t}+\frac{\partial \hat{\mathbf{F}}}{\partial x}\right)dx=\int_{x_i}^{x_{i+1}} W\hat{\mathbf{S}}dx \qquad 3\text{-}14$$

In Galerkin finite element method, the weighting function $W(x)$ is taken the same as interpolation functions, after integrating by parts the following equation is obtained

$$\begin{gathered}\int_{x_i}^{x_{i+1}} N_i N_j dx\frac{\partial \mathbf{U}_j}{\partial t}-\int_{x_i}^{x_{i+1}}\frac{\partial N_i}{\partial x}\hat{\mathbf{F}}dx+N_i(x_{i+1})\hat{\mathbf{F}}(x_{i+1})- \\ N_i(x_i)\hat{\mathbf{F}}(x_i)=\int_{x_i}^{x_{i+1}} N_i\hat{\mathbf{S}}dx\end{gathered} \qquad 3\text{-}15$$

where $\hat{\mathbf{F}}(x,t)$ is the numerical flux across the element boundary.

The formulation for each component of $\hat{\mathbf{U}}$ can be written as

$$\int_{x_i}^{x_{i+1}} N_i N_j dx\frac{\partial U_j}{\partial t}-\int_{x_i}^{x_{i+1}}\frac{\partial N_i}{\partial x}\hat{F}dx+N_i(x_{i+1})\hat{F}(x_{i+1})-N_i(x_i)\hat{F}(x_i)=\int_{x_i}^{x_{i+1}} N_i\hat{S}dx \qquad 3\text{-}16$$

where *U*, *F* and *S* are the components of vectors $\mathbf{U}$, $\mathbf{F}$ and $\mathbf{S}$.

Approximate Riemann Solvers

Since the values across the element boundaries are discontinuous, the solution of the numerical flux across the boundary can be considered as Riemann problem. To compute the numerical flux for generalized Riemann problem, Harten et al. (1983) presented a novel approach to solve the Riemann problem approximately, known as HLL flux. Their approach assumed a two-wave configuration separating three constant states. In addition, by assuming the wave velocities as known, the integration over the conservation laws gave the approximate solution for numerical flux.

As the one dimensional shallow water equations are a two-wave system, the HLL flux should be accurate enough to calculate numerical flux. For systems having more than two waves (or more than two eigenvalues), like two dimensional shallow water equations, Toro et al. (1994) introduced a three-wave model to calculate numerical flux called HLLC flux function (C for contact wave).

HLL Flux

For homogeneous conservation laws of the form given below

$$\mathbf{U}_t + \mathbf{F}_x = 0 \qquad 3\text{-}17$$

The two-wave configuration is shown in Figure 3-2.

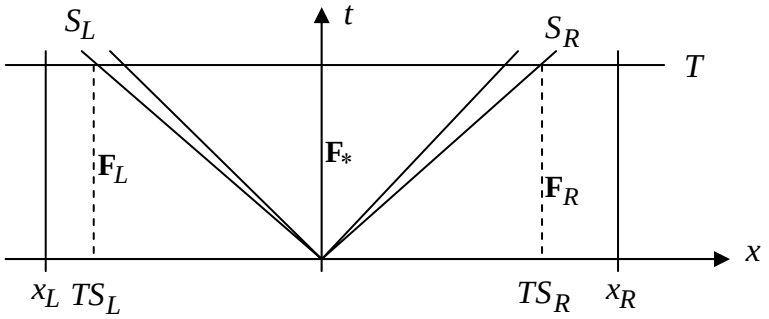

Figure 3-2. Two-wave configuration

where S_L and S_R are the fastest wave velocities, in terms of absolute value, arising from the solution of the Riemann problem.

By integrating the conservation laws over the control volume $[TS_L, 0]\times[0, T]$ in $x-t$ plane gives the following

$$\iint \left(\mathbf{U}_t + \mathbf{F}_x\right) dxdt = 0 \qquad 3\text{-}18$$

After applying Green's theorem (3-18) can be written as

$$\int_L \mathbf{U}dx - \mathbf{F}dt = 0 \tag{3-19}$$

$$(\mathbf{U}_L - \mathbf{U}_*)(0 - TS_L) - T(\mathbf{F}_* - \mathbf{F}_L) = 0 \tag{3-20}$$

where $\mathbf{F}_L$, $\mathbf{F}_R$, and $\mathbf{F}_*$ are numerical fluxes across the boundary.

In the same way, integrating the conservation laws over the control volume $[0, TS_R] \times [0, T]$ gives the following equation

$$(\mathbf{U}_R - \mathbf{U}_*)(TS_R - 0) - T(\mathbf{F}_R - \mathbf{F}_*) = 0 \tag{3-21}$$

Equations (3-20) and (3-21) can be written as (3-22) and (3-23), respectively

$$\mathbf{U}_* = \mathbf{U}_L + \frac{T(\mathbf{F}_* - \mathbf{F}_L)}{TS_L} \tag{3-22}$$

$$\mathbf{U}_* = \mathbf{U}_R - \frac{T(\mathbf{F}_R - \mathbf{F}_*)}{TS_R} \tag{3-23}$$

Equations (3-22) and (3-23) result in the following

$$\mathbf{F}_* = \frac{S_R\mathbf{F}_L - S_L\mathbf{F}_R + S_L S_R(\mathbf{U}_R - \mathbf{U}_L)}{S_R - S_L} \tag{3-24}$$

The trivial cases of $S_L \geq 0$ and $S_R \leq 0$ can be observed from wave configuration. Thus, the HLL flux for approximate Riemann problem is given by

$$\mathbf{F}^{HLL} = \begin{cases} \mathbf{F}_L & \text{if } S_L \geq 0 \\ \dfrac{S_R\mathbf{F}_L - S_L\mathbf{F}_R + S_L S_R(\mathbf{U}_R - \mathbf{U}_L)}{S_R - S_L}, & \text{if } S_L \leq 0 \leq S_R \\ \mathbf{F}_R & \text{if } S_R \leq 0 \end{cases} \tag{3-25}$$

The wave speeds, S_L and S_R, are required for the calculation of HLL flux. For the one dimensional shallow water equations, a direct way to calculate wave speeds across the discontinuous element boundary is:

$$S_L = \min\left(u^- - \sqrt{gh^-}, u^+ - \sqrt{gh^+}\right), \quad S_R = \max\left(u^- + \sqrt{gh^-}, u^+ + \sqrt{gh^+}\right) \qquad 3\text{-}26$$

Fraccarollo and Toro (1995) suggested the following equations to estimated wave speeds

$$S_L = \min(u^- - \sqrt{gh^-}, u^* - \sqrt{gh^*}) \qquad 3\text{-}27$$

$$S_R = \max(u^+ + \sqrt{gh^+}, u^* + \sqrt{gh^*}) \qquad 3\text{-}28$$

where

$$u^* = \frac{1}{2}(u^- + u^+) + \sqrt{gh^-} - \sqrt{gh^+} \qquad 3\text{-}29$$

$$\sqrt{gh^*} = \frac{1}{2}\left(\sqrt{gh^-} + \sqrt{gh^+}\right) + \frac{1}{4}\left(u^- - u^+\right) \qquad 3\text{-}30$$

If $S_{\max}$ is defined as

$$S_{\max} = \max\left(\left|u^-\right| + \sqrt{gh^-}, \left|u^+\right| + \sqrt{gh^+}\right) \qquad 3\text{-}31$$

then $S_L = -S_{\max}$ and $S_R = S_{\max}$.

This will result in the Lax-Friedrichs flux and is given by

$$\mathbf{F}^{LF} = \frac{1}{2}\left(\mathbf{F}^- + \mathbf{F}^+\right) - S_{\max}(\mathbf{U}^+ - \mathbf{U}^-) \qquad 3\text{-}32$$

Einfeldt (1988) proposed to estimate wave speeds with Roe's eigenvalues as follows

$$S_L = \tilde{u} - \tilde{c}, \; S_R = \tilde{u} + \tilde{c} \qquad 3\text{-}33$$

where

$$\tilde{u} = \frac{\sqrt{h^-}u^- + \sqrt{h^+}u^+}{\sqrt{h^-} + \sqrt{h^+}} \tag{3-34}$$

$$\tilde{c} = \sqrt{\frac{g\left(h^- + h^+\right)}{2}} \tag{3-35}$$

and the approach is called HLLE.

Roe's Flux

Besides the HLL type approximate Riemann solver, the Roe flux function may be the most well-known and widely used approximate Riemann solver. For the conservation laws, the Jacobian matrix is given by

$$\mathbf{A}(\mathbf{U}) = \frac{\partial \mathbf{F}}{\partial \mathbf{U}} \tag{3-36}$$

and the conservation laws can be written as

$$\mathbf{U}_t + \mathbf{A}(\mathbf{U})\mathbf{U}_x = 0 \tag{3-37}$$

The original Jacobian matrix $\left(\mathbf{A}\right)$ is replaced by a constant Jacobian matrix $\left(\tilde{\mathbf{A}}\right)$ as follows

$$\tilde{\mathbf{A}} = \mathbf{A}(\mathbf{U}_L, \mathbf{U}_R) \tag{3-38}$$

The original nonlinear system of conservation laws becomes a linear system with constant coefficients and is given by

$$\mathbf{U}_t + \tilde{\mathbf{A}}\mathbf{U}_x = 0 \tag{3-39}$$

or

$$\mathbf{U}_t + \tilde{\mathbf{F}}_x = 0 \tag{3-40}$$

The solution to the linear system at an interior node (as shown in Figure 3-2) is given by

$$\mathbf{U}(x=0,t) = \mathbf{U}_L + \sum_{\tilde{\lambda}_i \le 0} \tilde{\alpha}_i \tilde{\mathbf{k}}_i \tag{3-41}$$

or

$$\mathbf{U}(x=0,t) = \mathbf{U}_R - \sum_{\tilde{\lambda}_i \ge 0} \tilde{\alpha}_i \tilde{\mathbf{k}}_i \tag{3-42}$$

where $\tilde{\lambda}_i$ are eigenvalues of $\tilde{\mathbf{A}}$ and $\tilde{\alpha}_i = \tilde{\alpha}_i(\mathbf{U}_L, \mathbf{U}_R)$ are the wave strengths and will be defined later. Equations (3-41) and (3-42) are combined to obtain the following equation

$$\mathbf{U}_R - \mathbf{U}_L = \sum_{i=1}^{m} \tilde{\alpha}_i \tilde{\mathbf{k}}_i \tag{3-43}$$

where m is the number of eigenvalues of the conservation Law.

Applying Green's theorem gives the numerical flux for the original conservational laws as

$$\mathbf{F}^* = \mathbf{F}_L - S_L \mathbf{U}_L - \frac{1}{T} \int_{TS_L}^{0} \mathbf{U} dx \tag{3-44}$$

or

$$\mathbf{F}^* = \mathbf{F}_R - S_R \mathbf{U}_R + \frac{1}{T} \int_{0}^{TS_R} \mathbf{U} dx \tag{3-45}$$

While the numerical flux for the linearized system is given by

$$\tilde{\mathbf{F}}^{*} = \tilde{\mathbf{F}}_L - S_L \mathbf{U}_L - \frac{1}{T}\int_{TS_L}^{0} \tilde{\mathbf{U}} dx \qquad 3\text{-}46$$

or

$$\tilde{\mathbf{F}}^{*} = \tilde{\mathbf{F}}_R - S_R \mathbf{U}_R + \frac{1}{T}\int_{0}^{TS_R} \tilde{\mathbf{U}} dx \qquad 3\text{-}47$$

With the following approximation

$$\int_{TS_L}^{0} \mathbf{U} dx = \int_{TS_L}^{0} \tilde{\mathbf{U}} dx \qquad 3\text{-}48$$

$$\int_{0}^{TS_R} \mathbf{U} dx = \int_{0}^{TS_R} \tilde{\mathbf{U}} dx \qquad 3\text{-}49$$

$$\tilde{\mathbf{F}}(\mathbf{U}) = \tilde{\mathbf{A}}\mathbf{U} \qquad 3\text{-}50$$

Equations (3-46) and (3-47) are then combined to determine the Roe numerical flux across the boundary and is given by

$$\mathbf{F}^{Roe} = \frac{1}{2}(\mathbf{F}_L + \mathbf{F}_R) - \frac{1}{2}\sum_{i=1}^{m} \tilde{\alpha}_i \left|\tilde{\lambda}_i\right| \tilde{\mathbf{k}}_i \qquad 3\text{-}51$$

The Roe's Jacobian matrix is required to satisfy the following properties:

(1) provide a linear mapping from the space **U** to **F**;

(2) show consistency with exact Jacobian matrix

$$\tilde{\mathbf{A}}(\mathbf{U}_L = \mathbf{U}_R) = \mathbf{A}(\mathbf{U}) \qquad 3\text{-}52$$

(3) offer conservation across discontinuities

$$\mathbf{F}(\mathbf{U_R}) - \mathbf{F}(\mathbf{U_L}) = \tilde{\mathbf{A}} \times (\mathbf{U_R} - \mathbf{U_L}) \qquad 3\text{-}53$$

(4) the eigenvectors of $\tilde{\mathbf{A}}$ be linearly independent.

The Roe's flux function for one dimensional shallow water flow is given across the discontinuous element boundary as

$$\mathbf{F}^{Roe} = \frac{1}{2}\left(\mathbf{F}^{-} + \mathbf{F}^{+}\right) - \frac{1}{2}\sum_{i=1}^{2} \tilde{\alpha}_i \left|\tilde{\lambda}_i\right| \tilde{\mathbf{k}}_i \qquad 3\text{-}54$$

where

$$\tilde{\alpha}_1 = \frac{1}{2}\left(\Delta h - \frac{\tilde{h}\Delta u}{\tilde{c}}\right), \quad \tilde{\alpha}_2 = \frac{1}{2}\left(\Delta h + \frac{\tilde{h}\Delta u}{\tilde{c}}\right) \qquad 3\text{-}55$$

$$\tilde{\lambda}_1 = \tilde{u} - \tilde{c}, \quad \tilde{\lambda}_2 = \tilde{u} + \tilde{c} \qquad 3\text{-}56$$

$$\tilde{\mathbf{k}}_1 = \left[1, \tilde{u} - \tilde{c}\right]^T, \quad \tilde{\mathbf{k}}_2 = \left[1, \tilde{u} + \tilde{c}\right]^T \qquad 3\text{-}57$$

$$\Delta h = h^+ - h^-, \quad \Delta u = u^+ - u^- \qquad 3\text{-}58$$

$$\tilde{h} = \sqrt{h^- h^+} \qquad 3\text{-}59$$

$$\tilde{u} = \frac{\sqrt{h^-}u^- + \sqrt{h^+}u^+}{\sqrt{h^-} + \sqrt{h^+}} \qquad 3\text{-}60$$

$$\tilde{c} = \sqrt{\frac{g\left(h^- + h^+\right)}{2}} \qquad 3\text{-}61$$

Time integration

The TVD Runge-Kutta time integration scheme should be one order higher than the space discretization (Cockburn and Shu, 1989). For a general time dependent equation of the form given below

$$\frac{\partial \mathbf{U}}{\partial t} = L(\mathbf{U}) \tag{3-62}$$

Gottlieb and Shu (1998) proposed the following the second order TVD Runge-Kutta scheme

$$\begin{cases} \mathbf{U}^{[1]} = \mathbf{U}^n + \Delta t L(\mathbf{U}^n) \\ \mathbf{U}^{n+1} = \frac{1}{2}\mathbf{U}^n + \frac{1}{2}\mathbf{U}^{[1]} + \frac{1}{2}\Delta t L(\mathbf{U}^{[1]}) \end{cases} \tag{3-63}$$

and a third order TVD Runge-Kutta scheme was also proposed and is shown below

$$\begin{cases} \mathbf{U}^{[1]} = \mathbf{U}^n + \Delta t L(\mathbf{U}^n) \\ \mathbf{U}^{[2]} = \frac{3}{4}\mathbf{U}^n + \frac{1}{4}\mathbf{U}^{[1]} + \frac{1}{4}\Delta t L(\mathbf{U}^{[1]}) \\ \mathbf{U}^{n+1} = \frac{1}{3}\mathbf{U}^n + \frac{2}{3}\mathbf{U}^{[2]} + \frac{2}{3}\Delta t L(\mathbf{U}^{[2]}) \end{cases} \tag{3-64}$$

For the explicit scheme, the Courant-Friedrichs-Lewy condition is required for the stability and is given by

$$\max[\frac{\Delta t}{\Delta x}(|u| + c)] \le \frac{1}{2r+1} \tag{3-65}$$

where r is the order of polynomials for space discretization (CockBurn B. 2001).

Slope limiter

To achieve TVD property in a numerical scheme, flux limiters and slope limiters are often applied in combination with TVD time integration. Here the slope limiter is adopted. Instead of applying the slope limiter on conserved variable flow depth, the slope limiter is applied on water surface as well as flow rate. And the effect of slope limiter on water surface and water depth will be compared.

In an element j, the application of water surface slope limiter can be written as

$$\tilde{Z}(x) = \overline{Z}(x) + (x - x_m)\sigma_j, \quad x_1 < x < x_2 \tag{3-66}$$

where

$$Z = z_b + h \quad \text{and} \quad x_m = \left(x_1 + x_2\right)/2 \tag{3-67}$$

and the average bed elevation $\overline{Z}$ is given by

$$\overline{Z}(x) = \frac{1}{(x_2 - x_1)} \int_{x_1}^{x_2} Z(x)dx \tag{3-68}$$

Slope limiters reported that satisfy the TVD condition include following different forms: (Li 2006).

For Godunov method

$$\sigma_j = 0 \tag{3-69}$$

while the minmod slope limiter is given by

$$\sigma_j = sign(a,b)\min(|a|,|b|) \tag{3-70}$$

and monotonized central slope limiter can be written as

$$\sigma_j = sign(a,b)\min(\frac{|a+b|}{2}, 2|a|, 2|b|) \tag{3-71}$$

where the upwind slope, downwind, and central slope are given, respectively, by

$$a = \frac{\overline{Z}_j - \overline{Z}_{j-1}}{(x_{j,m} - x_{j-1,m})} \tag{3-72}$$

$$b = \frac{\overline{Z}_{j+1} - \overline{Z}_j}{(x_{j+1,m} - x_{j,m})} \tag{3-73}$$

$$\frac{a+b}{2} = \frac{\overline{Z}_{j+1} - \overline{Z}_{j-1}}{2(x_{j+1,m} - x_{j-1,m})} \qquad 3\text{-}74$$

where $\overline{Z}_j$ is the average water level of element j and $x_{j,m}$ is the midpoint of element j.

CHAPTER FOUR

NUMERICAL TESTS

A number of numerical tests are conducted to investigate the proposed numerical scheme for one-dimensional shallow water flows with and without bed variation. For horizontal bed, the water surface slope limiter would be the same as water depth slope limiter. These tests will be used to examine the applicability of the discontinuous Galerkin method and the effect of different flux functions. For channel with bed variation, results with water surface slope limiter and water depth slope limiter are compared.

Test 1: Idealized Dambreak

In this test, a wide rectangular channel with a horizontal and frictionless bed was considered. The resulting governing equations reduced to conservation laws without source term. The channel was 1200 *m* in length. The dam was located at 500 *m* from upstream. Initially, the upstream water depth was 10 *m* and downstream water depth was set to 2 *m*. Wang et al. (2000) used this dam break problem to test TVD property of the proposed schemes. Results are shown in Figure 4-1 and Figure 4-2. The numerical solutions of water depth and flow rate are in good agreement with exact solutions. The results show that all three numerical flux functions are capable of capturing the shock within the domain.

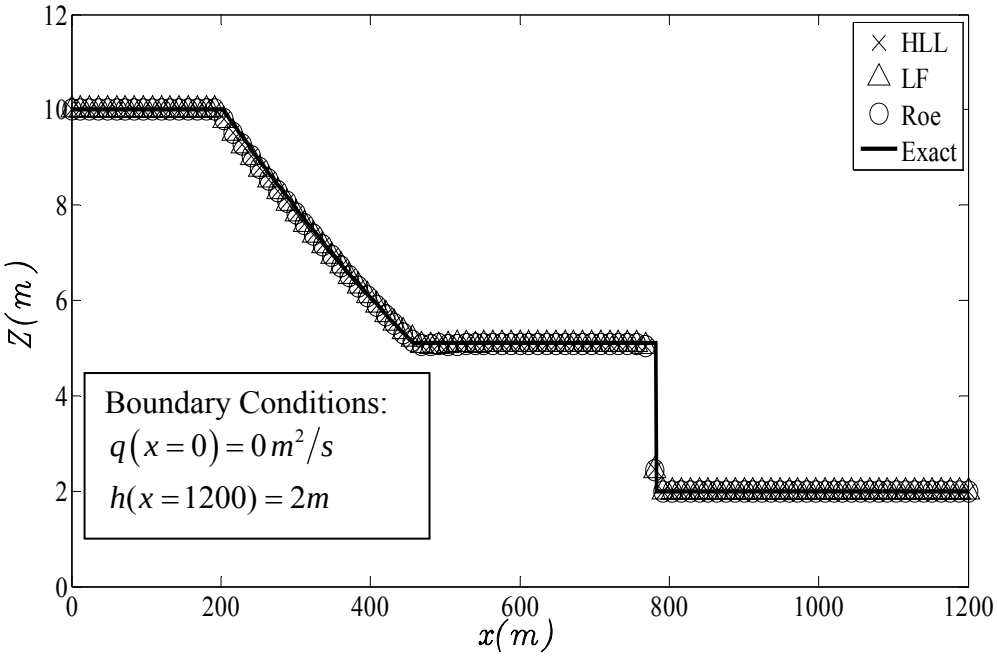

Figure 4-1. Numerical solution of water surface for ideal dambreak

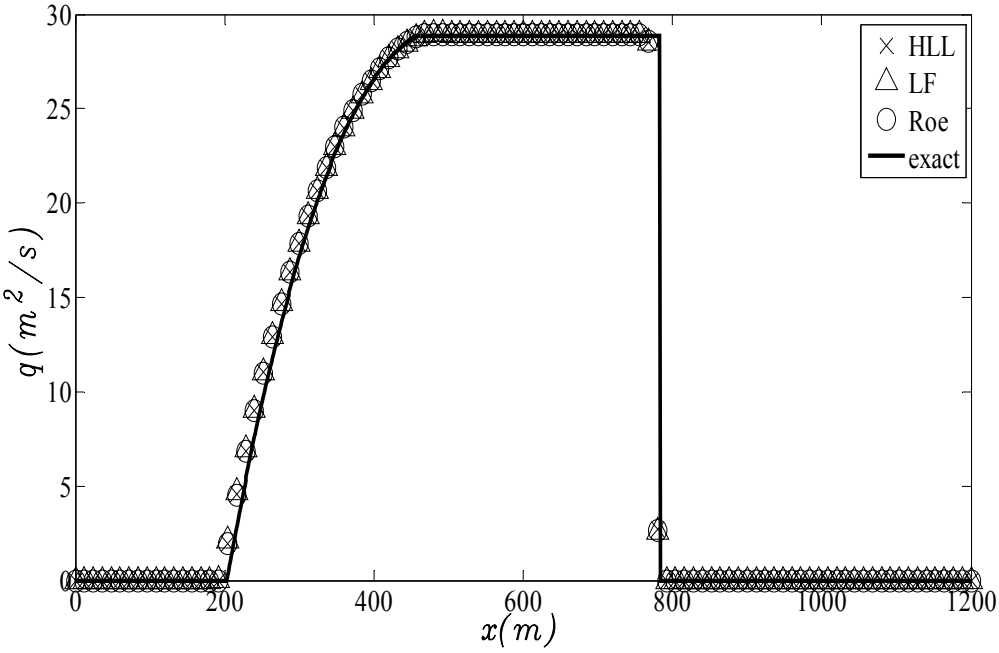

Figure 4-2. Numerical solution of flow rate for ideal dambreak

Test 2: Hydraulic Jump

Experimental data of hydraulic jump water surface profile collected by Gharangik and Chaudhry (1991) in a 14 *m* long and o.46 *m* wide flume was utilized in this test. Manning's coefficient was taken to be 0.008 $s/m^{1/3}$, so the resulting governing equations would represent conservation laws with source term due to friction only. Water depth was initially set to 0.031 *m*. At the upstream boundary, water depth of 0.031 *m* and discharge of 0.118 m^2/s were set, while the water depth at the downstream boundary was increased from 0.031 *m* to 0.265 *m* in 50 seconds. Results are shown in Figure 4-3 and Figure 4-4. The numerical solutions are capable of capturing shocks and preserve the conservative property. The LF flux function results in water surface and discharge oscillations at the jump location. The Roe flux and HLL functions result in oscillation-free water surface profile while the Roe flux function shows the best mass conservation property.

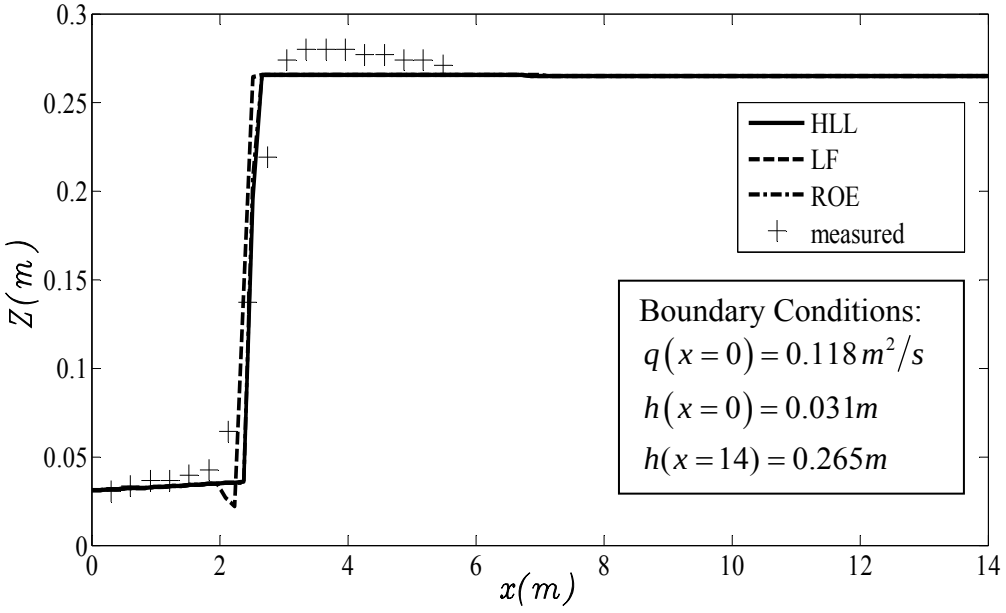

Figure 4-3. Numerical solution of water surface for hydraulic jump

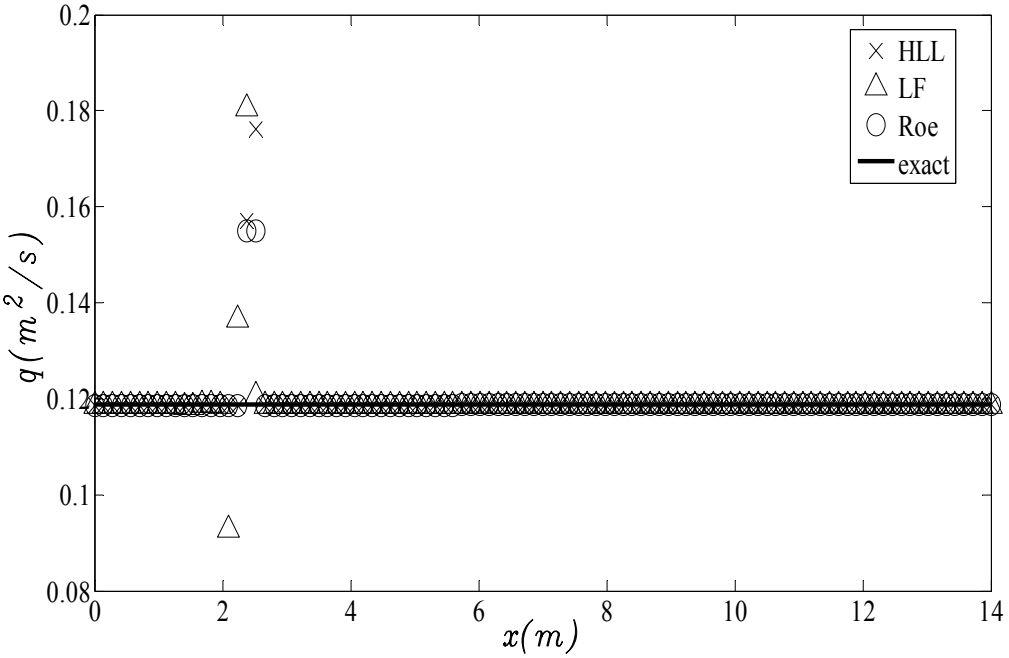

Figure 4-4. Numerical solution of flow rate for hydraulic jump

Test 3: Quiescent Water over a Bump

A frictionless 1 *m* wide 25 *m* long rectangular channel with a bump (Goutal and Maurel, 1997) given by Equation (4-1) is used for this test. The initial water depth is set to be 0.33 *m* and the flows in and out of the channel are set to be zero.

$$z_b = \begin{cases} 0.2 - 0.05(x-10)^2 & 8 \le x \le 12 \\ 0 \quad \text{otherwise} \end{cases} \qquad 4\text{-}1$$

Simulation results of water surface elevation and discharge per unit width, for the three different flux functions with the two slope limiters, are shown in Figure 4-5 to Figure 4-8. Numerical results show that when the water depth based slope limiter is used there are small oscillations in water depth and there is unphysical flow rate of the order of $10^{-3}\, m^2/s$. On the other hand, when the water surface based slope limiter is used, there are no water surface oscillations, and the oscillations in the flow rate drops to the order of $10^{-7}\, m^2/s$. In addition, for each of the slope limiter, the three different flux functions give results of the same order of accuracy.

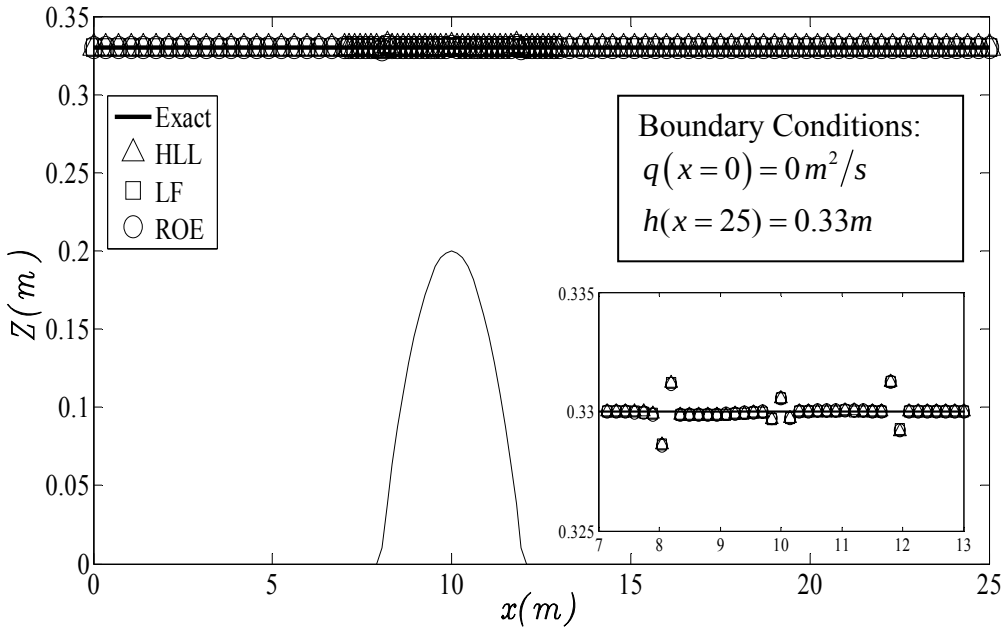

Figure 4-5. Numerical solution of water depth for Test 3 with water depth slope limiter

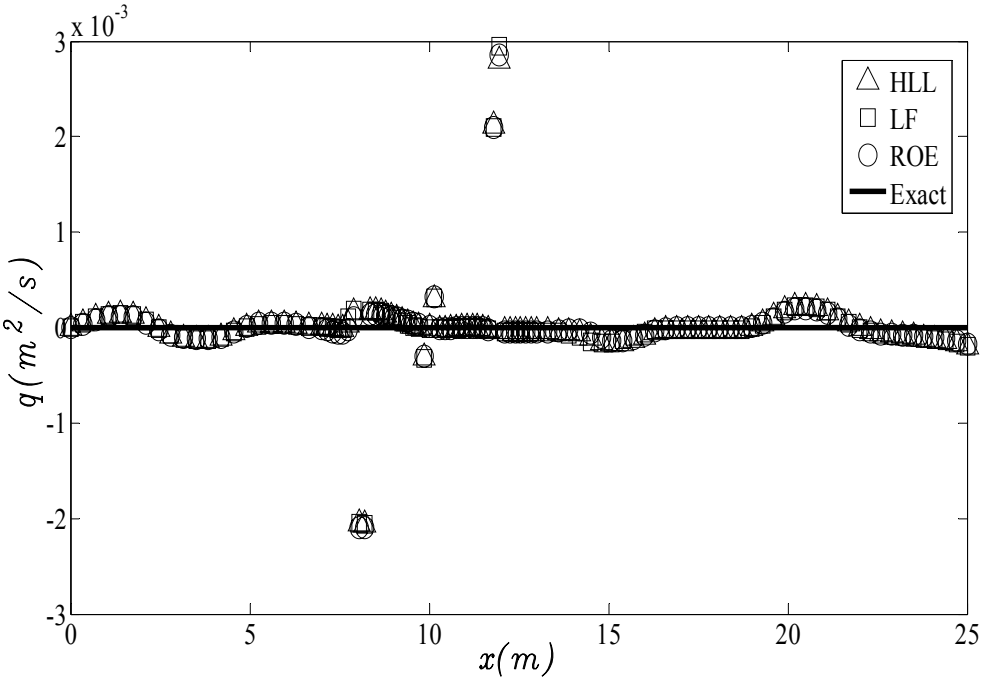

Figure 4-6. Numerical solution of flow rate for Test 3 with water depth slope limiter

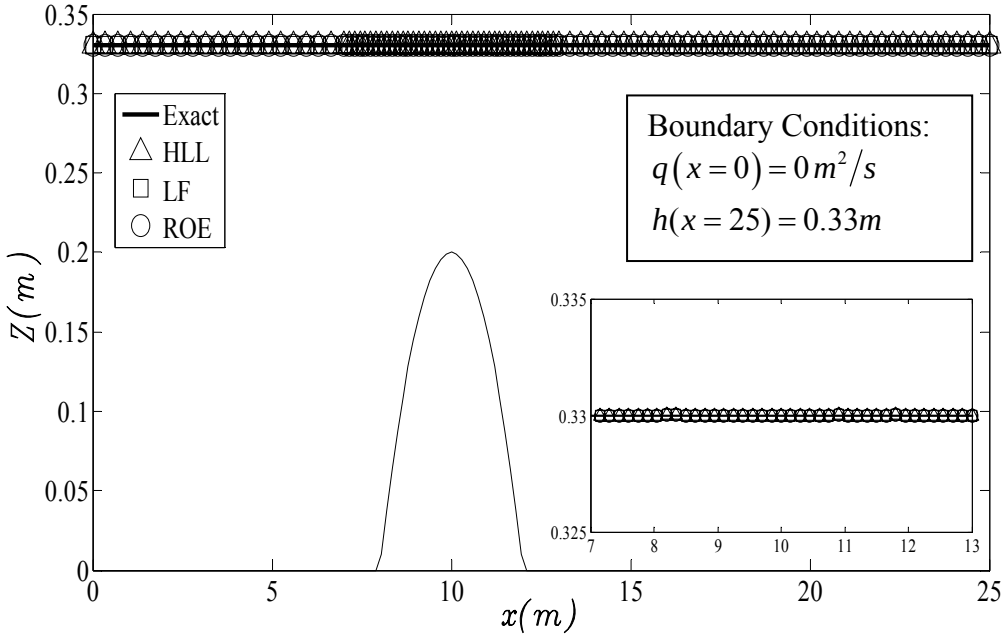

Figure 4-7. Numerical solution of water depth for Test 3 with water surface slope limiter

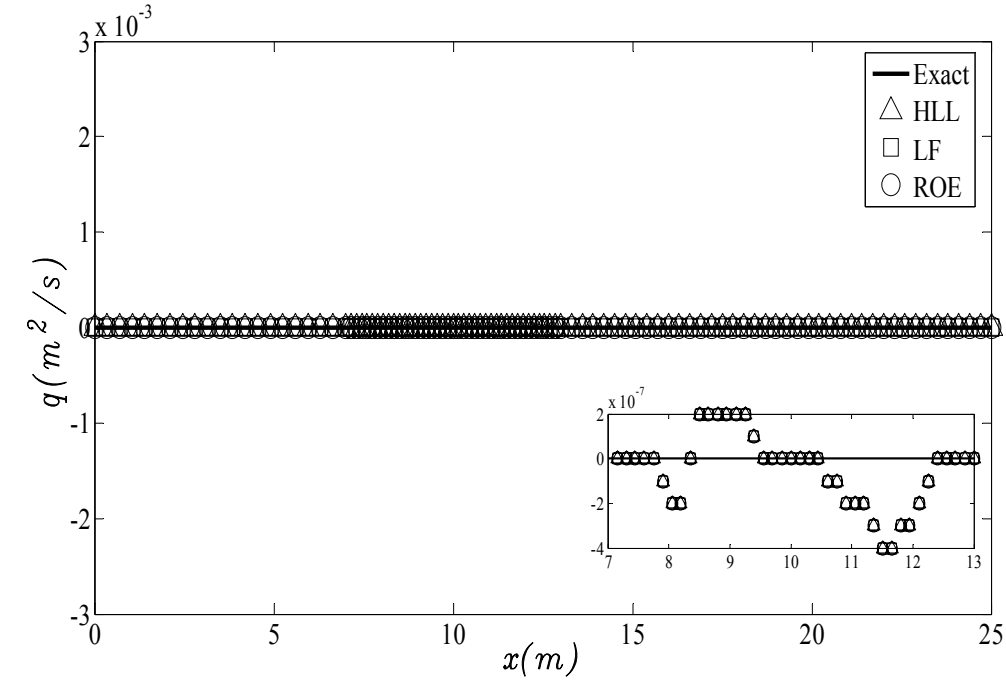

Figure 4-8. Numerical solution of flow rate for Test 3 with water surface slope limiter

Test 4: Subcritical Flow over a Bump

For this test, the channel width, length and bed elevation were as described as in Test 3. In this case, the flow rate at the inflow boundary was set to be 0.18 m^2/s and the downstream water surface elevation was set to 0.5 m. A subcritical flow condition exists throughout the channel.

The results of water surface and flow rate for the two slope limiters with three different flux approximations in each case are shown in Figure 4-9 to Figure 4-12. The water surface result shows oscillatory solution at the beginning and end of the bump for all three flux functions with water depth slope limiter. The water surface is predicted accurately with all three flux functions using the water surface slope limiter. The results for flow rate in case of water depth slope limiter show large oscillations over the bump. However, the water surface slope limiter preserves the conservation property.

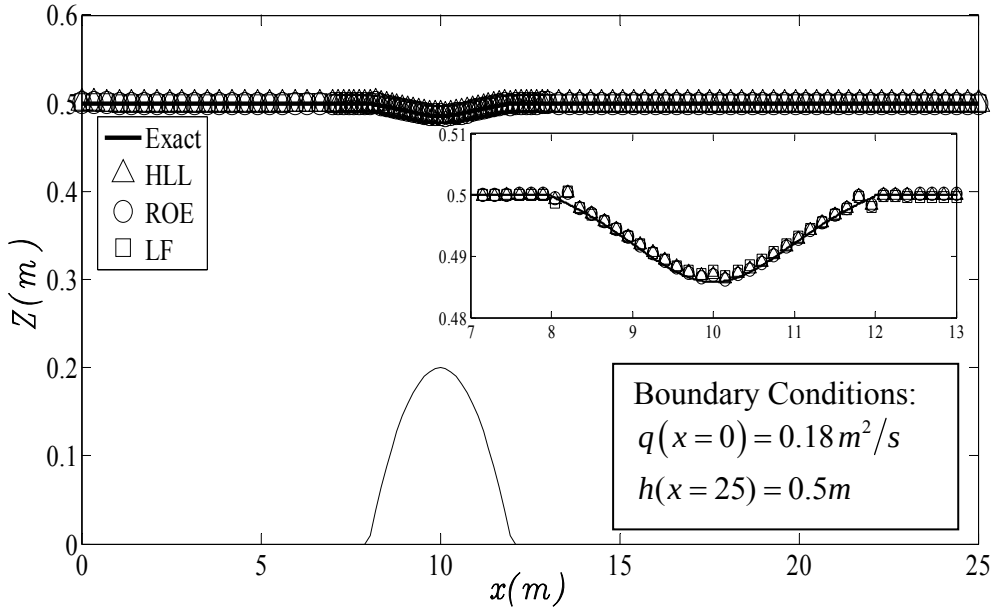

Figure 4-9. Numerical solution of water depth for Test 4 with water depth slope limiter

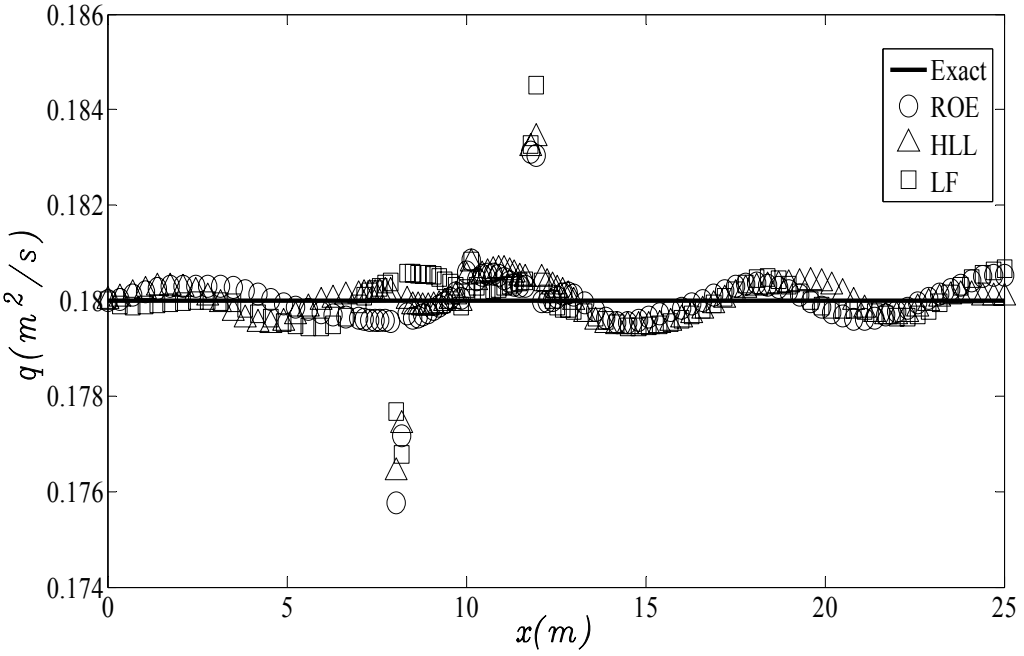

Figure 4-10. Numerical solution of flow rate for Test 4 with water depth slope limiter

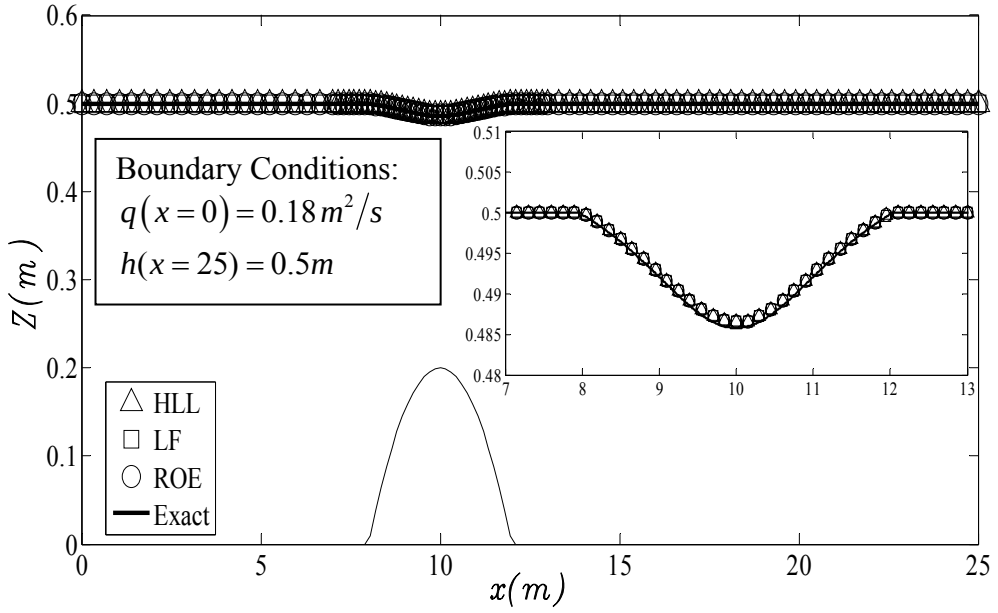

Figure 4-11. Numerical solution of water depth for Test 4 with water surface slope limiter

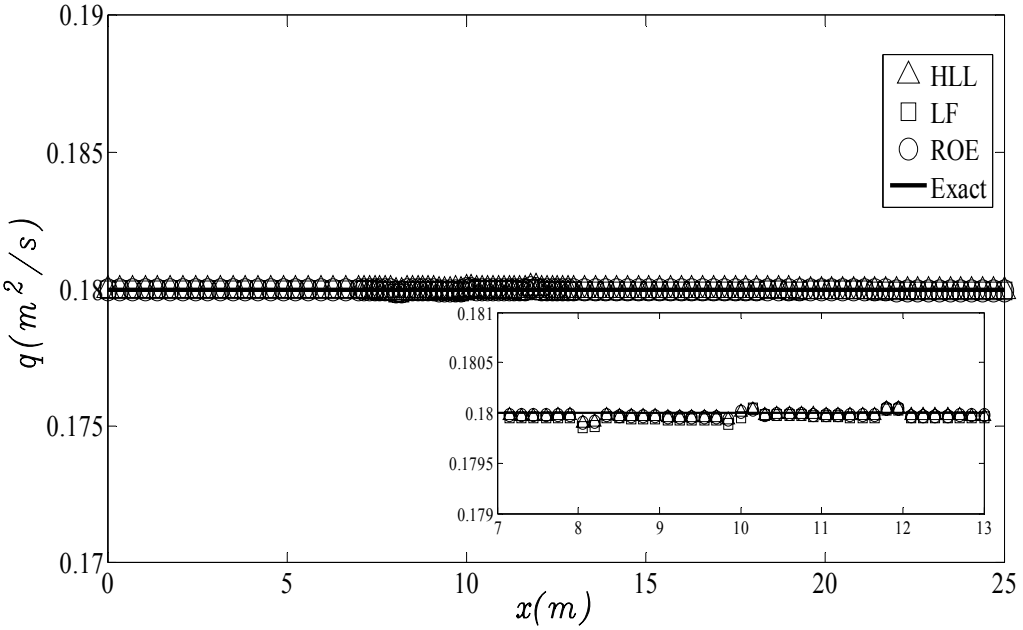

Figure 4-12. Numerical solution of flow rate for Test 4 with water surface slope limiter

Test 5: Transcritical Flow over a Bump

The channel width, length, and bed topography were as described for the previous two tests. Inflow boundary condition was set to $0.18 m^2/s$ and downstream water surface elevation was fixed at 0.33 *m*. Within the solution domain, the flow regime changed from subcritical to supercritical and back to subcritical flow through a hydraulic jump.

The numerical results for this test are shown in Figure 4-13 to Figure 4-16. In the figures, the solid line shows the analytical solution of the problem. The water surface level is predicted accurately by both slope limiters using the three different flux functions. As before, the simulation results of water surface based slope limiter provide better conservation properties for discharge than the water depth based slope limiter. Of the three flux functions, Roe flux conserves the flow rate most accurately and when used with water surface based flow limiter the discharge is constant throughout the domain.

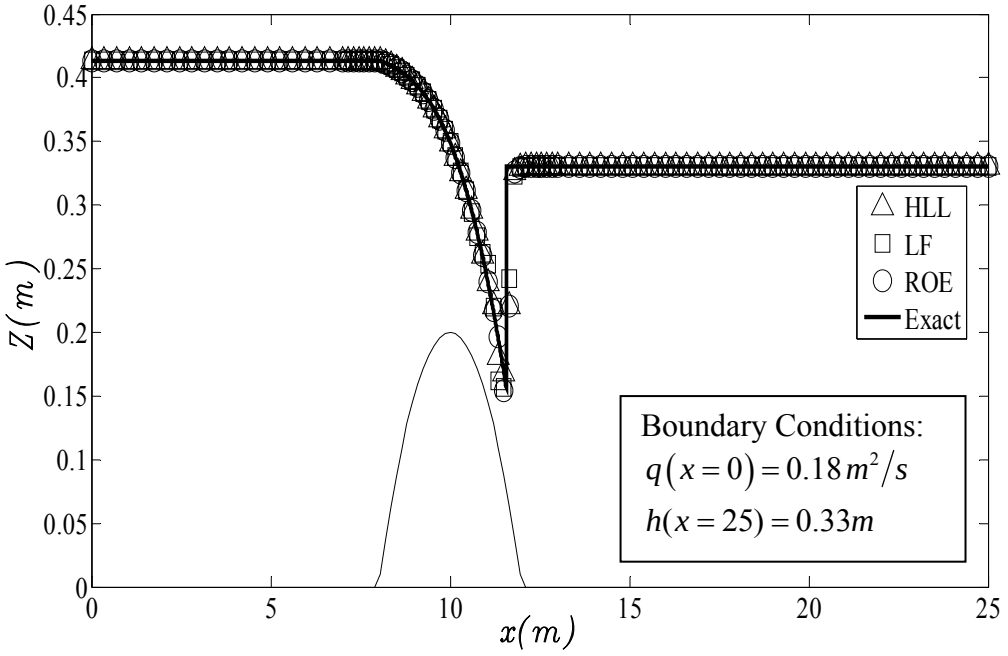

Figure 4-13. Numerical solution of water depth for Test 5 with water depth slope limiter

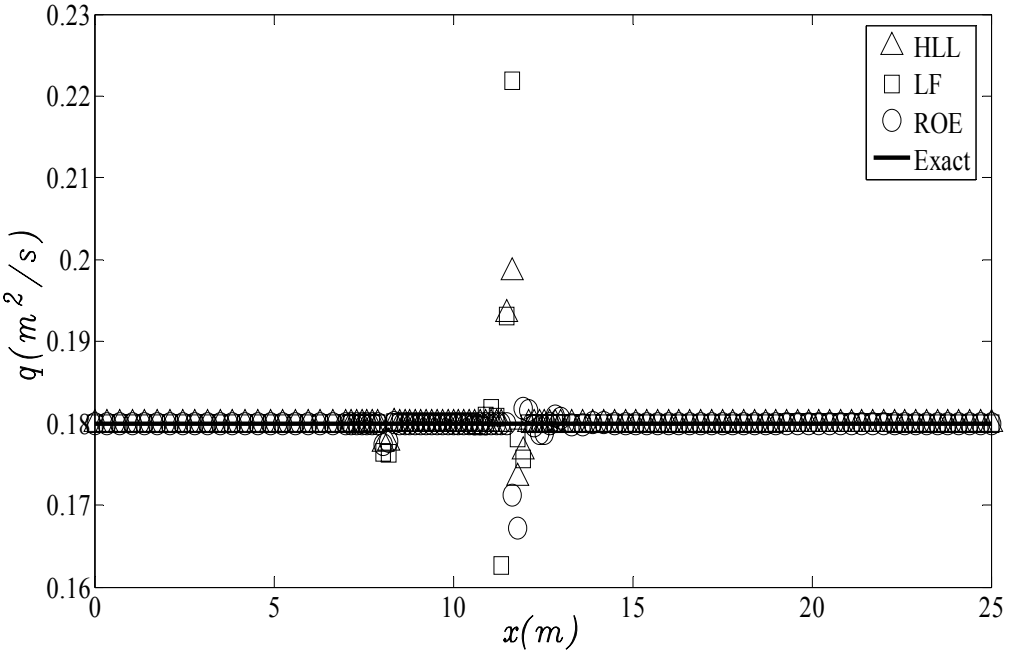

Figure 4-14. Numerical solution of flow rate for Test 5 with water depth slope limiter

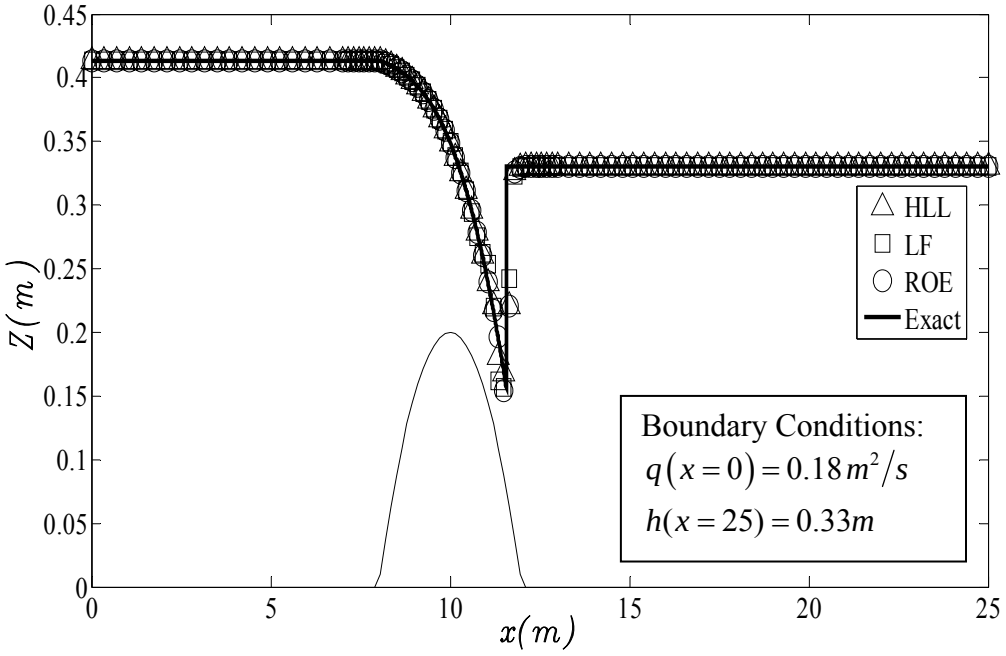

Figure 4-15. Numerical solution of water depth for Test 5 with water surface slope limiter

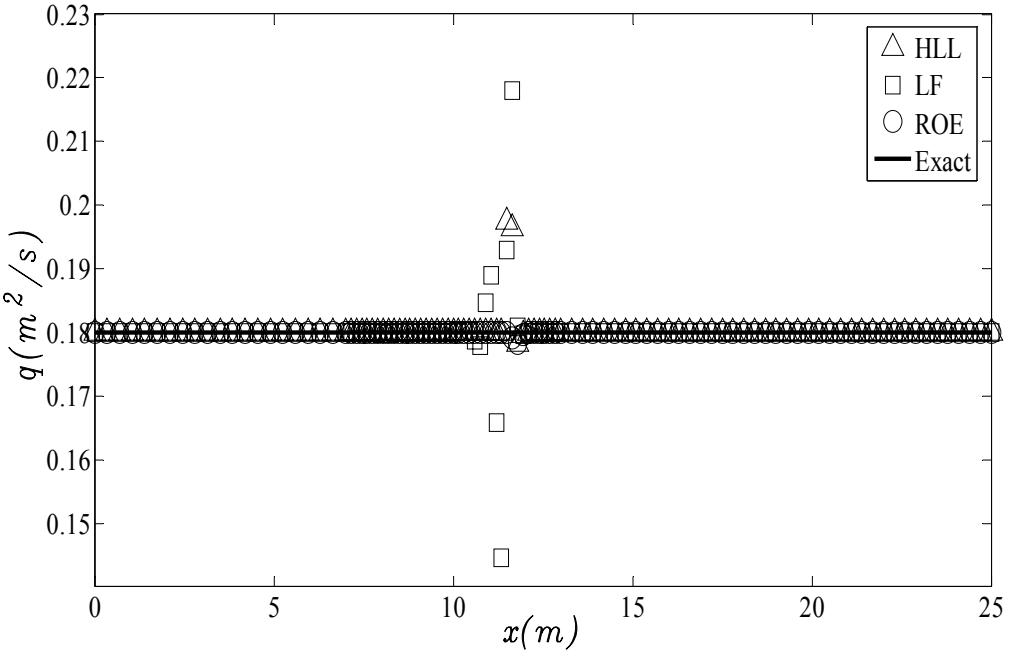

Figure 4-16. Numerical solution of flow rate for Test 5 with water surface slope limiter

Test 6: Supercritical Flow over a Bump

In this test, the channel geometry and bed topography was set as described for the previous test cases. The inflow discharge per unit width and flow depth at the upstream end was set to 25.0567 m^2/s and 2 m, respectively. The flow is supercritical throughout the domain.

The simulation results of water surface and discharge are shown in Figure 4-17 to Figure 4-20. The water depth is predicted accurately by the two slope limiter schemes with all three flux functions. The flow rate is preserved accurately by HLL and Roe flux functions with either slope limiter scheme. However for both slope limiters, the LF flux function gives unphysical oscillations for flow rate.

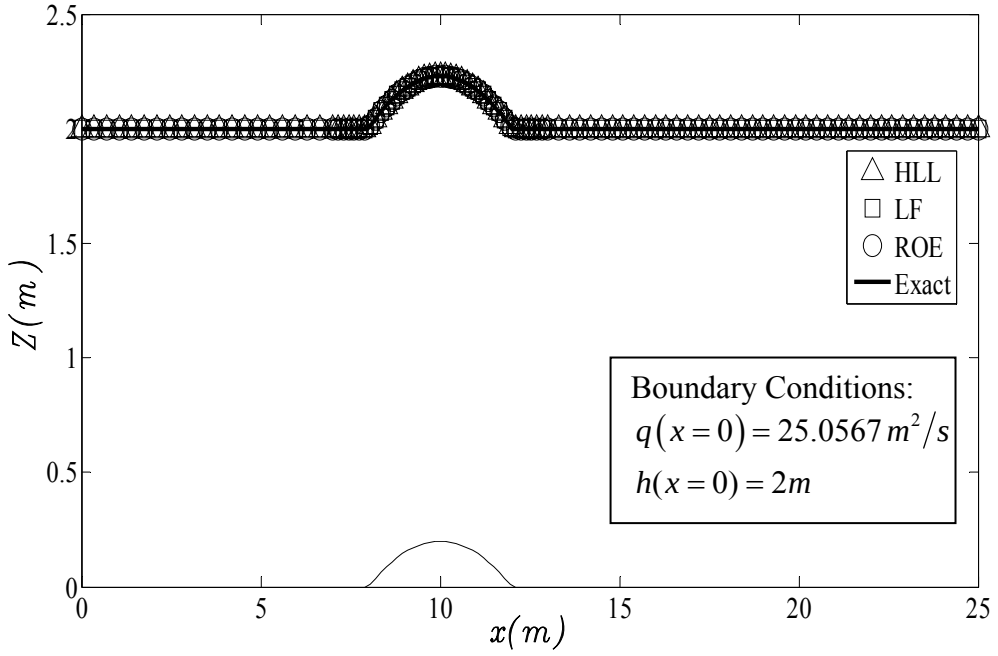

Figure 4-17. Numerical solution of water depth for Test 6 with water depth slope limiter

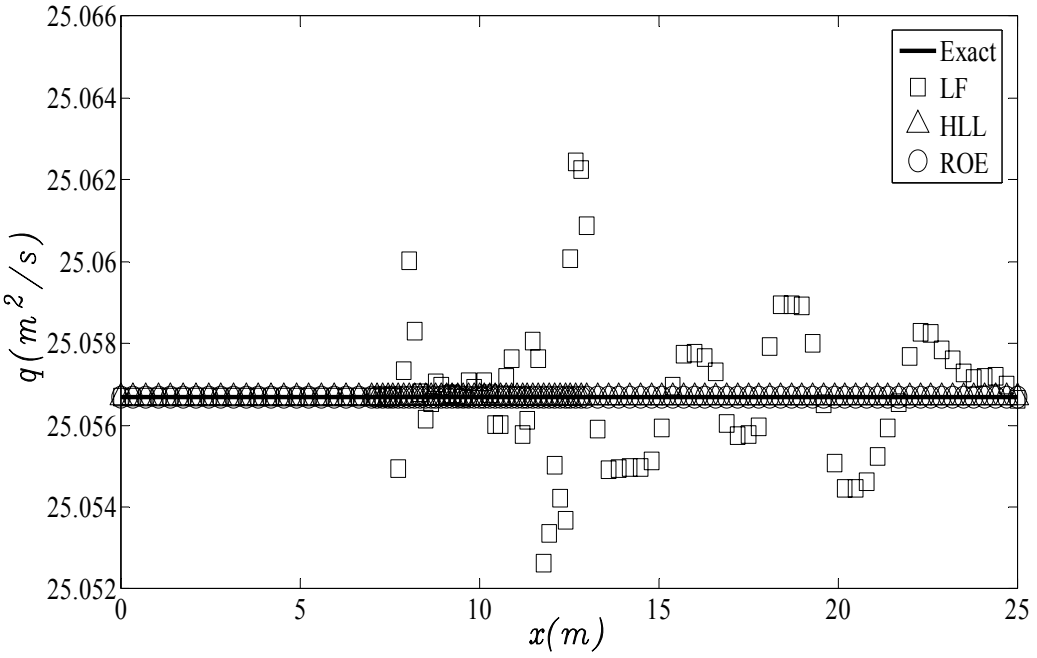

Figure 4-18. Numerical solution of flow rate for Test 6 with water depth slope limiter

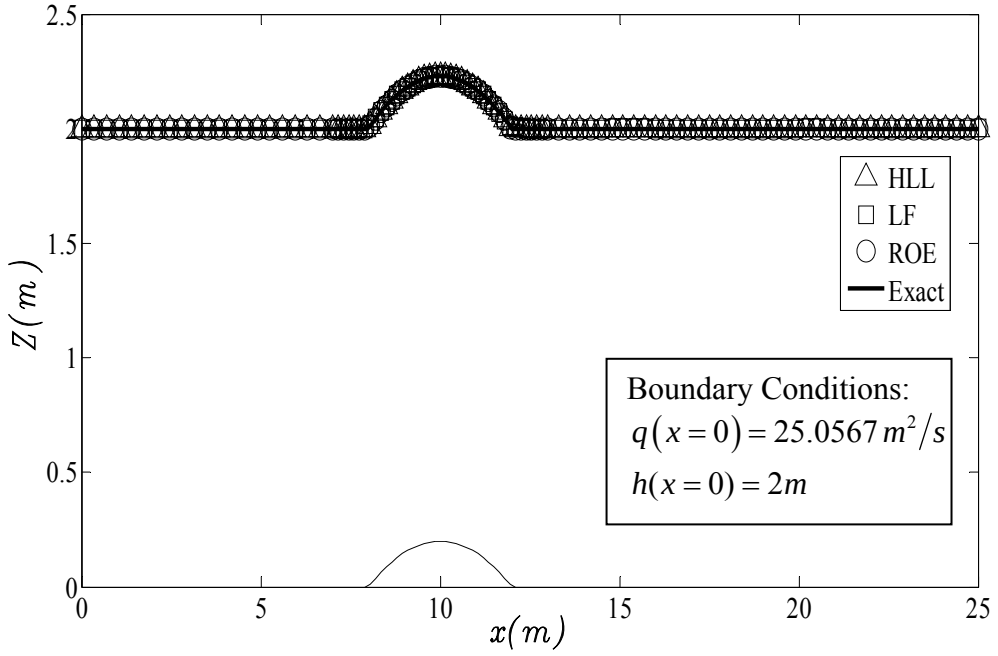

Figure 4-19. Numerical solution of water depth for Test 6 with water surface slope limiter

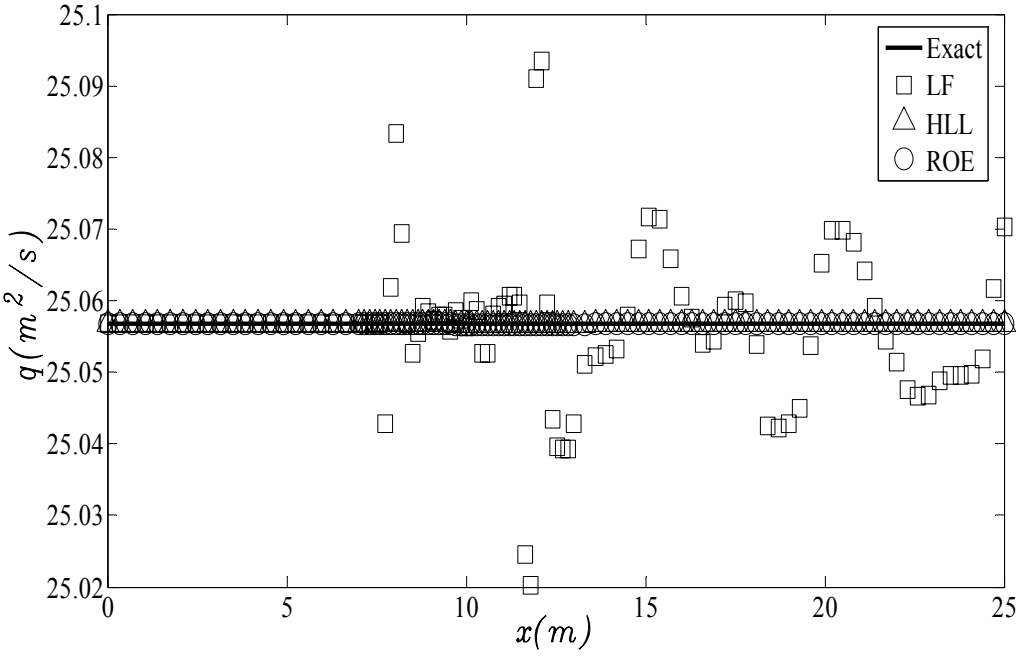

Figure 4-20. Numerical solution of flow rate for Test 6 with water surface slope limiter

Test 7: Quiescent Water over an Irregular Bed

In this test, a wide channel with bed topography (Goutal and Maurel, 1997) given in Table 4-1 was used. There was no flow in or out of the domain and the initial water surface level was set to 16 m. The aim was to evaluate the performance of the numerical schemes in suppressing unphysical flow and flow depth oscillations due to channel bed variation.

Table 4-1: Bed elevation (m) variation with distance (m)

x	0	50	100	150	200	250	300	350	400	425	435	450	470	475	500
z_b	0	0	2.5	5	5	3	5	5	7.5	8	9	9	9	9.1	9
x	505	530	550	565	575	600	650	700	750	800	820	900	950	1000	1500
z_b	9	6	5.5	5.5	5	4	3	3	2.3	2	1.2	0.4	0	0	0

The numerical results for water depth and flow rate are shown in Figure 4-21 to Figure 4-24. The results show the superiority of the slope limiter based on the water surface for preserving the initial condition of depth and zero flow rate for all three flux functions. In case of the slope limiter based on the water depth, the Roe flux function provides better results for maintaining the prescribed water depth and zero flow rate than other two flux functions.

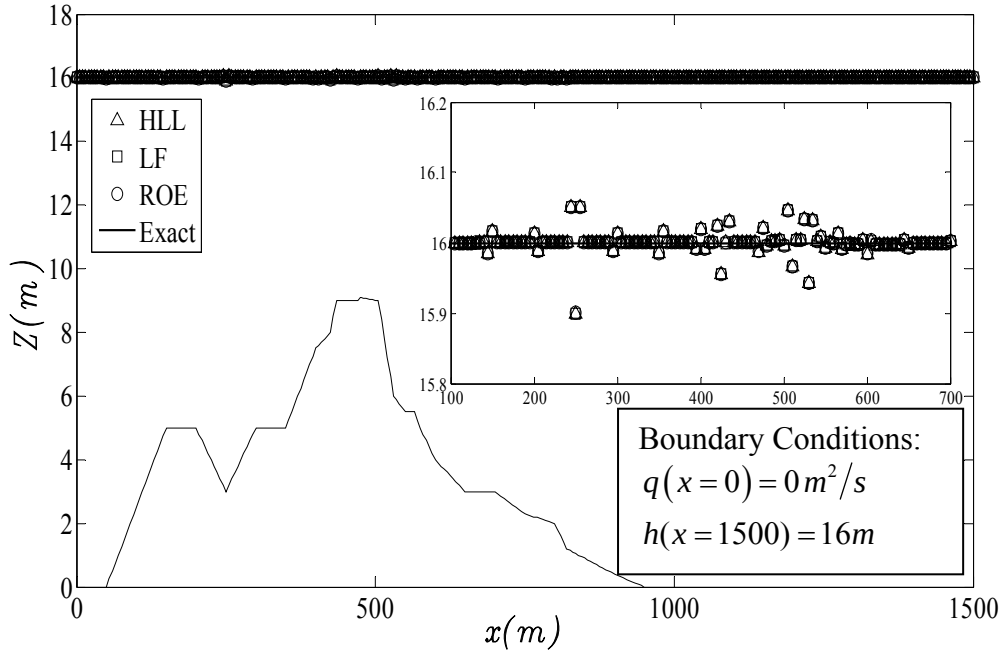

Figure 4-21. Numerical solution of water depth for Test 7 with water depth slope limiter

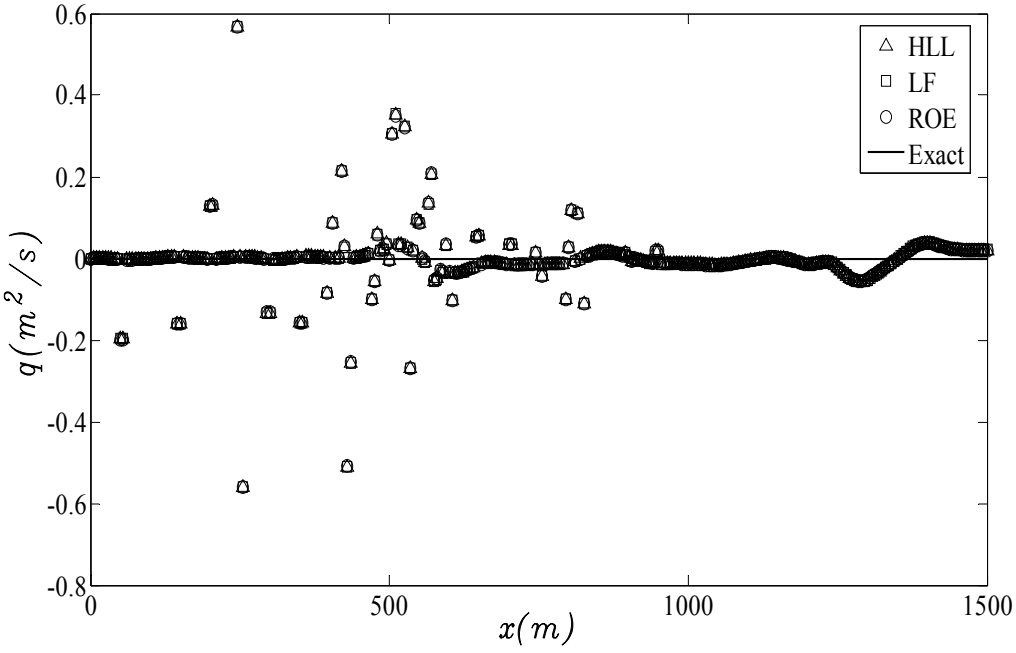

Figure 4-22. Numerical solution of flow rate for Test 7 with water depth slope limiter

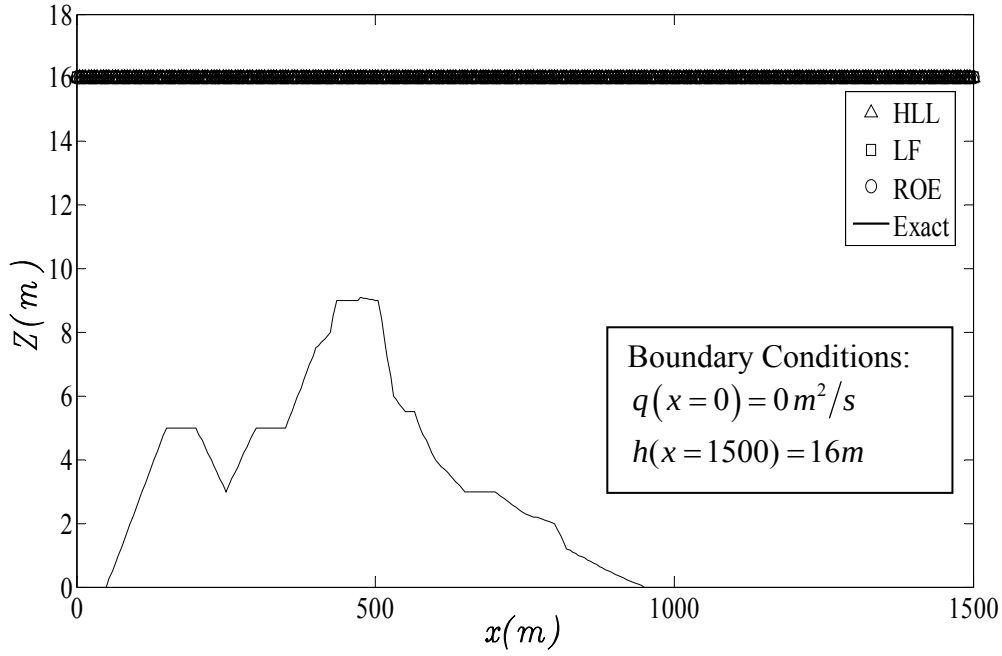

Figure 4-23. Numerical solution of water depth for Test 7 with water surface slope limiter

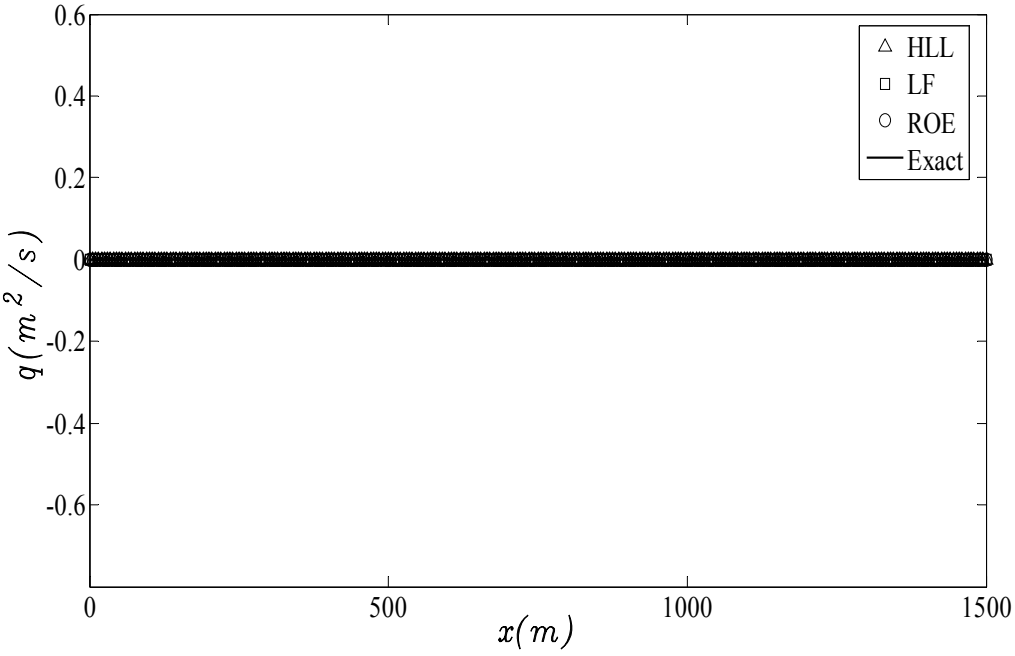

Figure 4-24. Numerical solution of flow rate for Test 7 with water surface slope limiter

Test 8: Subcritical Flow over an Irregular Bed

The channel with irregular bed, as described in the previous test, was used in this test. The inflow rate was set to 10 m^2/s and the downstream water depth was set to 16 *m.* The flow regime throughout the channel was subcritical.

The simulation results for the water depth and flow rate are shown in Figure 4-25 to Figure 4-28. The water surface level is predicted accurately by slope limiters based on the water surface and water depth with all three flux functions. However, the results for the flow rate exhibit oscillations in case of water depth based slope limiter. The LF flux provides the poorest results and the Roe flux the most accurate results. The water surface based slope limiter conserves the flow rate throughout the simulation domain. In this case also the Roe flux function provides the best results. A loss in flow rate is observed for the HLL and LF flux functions at the end of the channel.

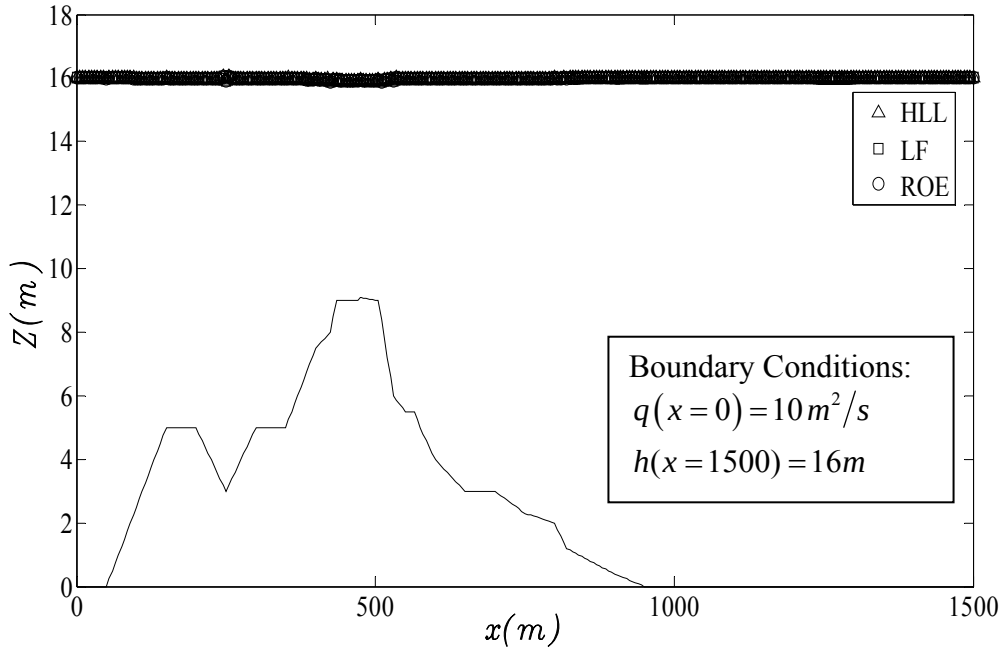

Figure 4-25. Numerical solution of water depth for Test 8 with water depth slope limiter

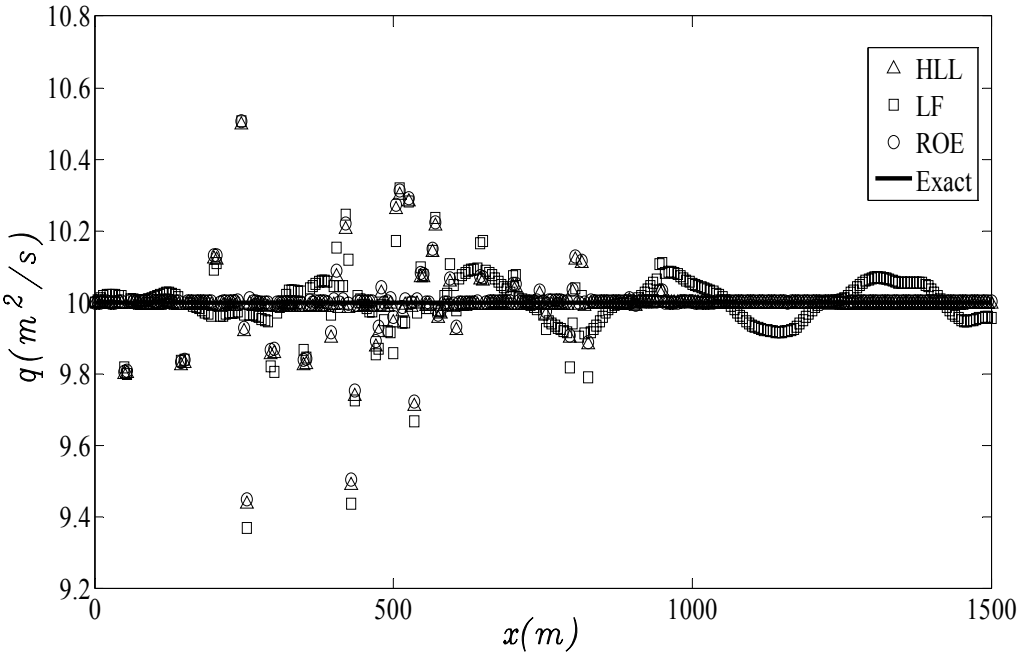

Figure 4-26. Numerical solution of flow rate for Test 8 with water depth slope limiter

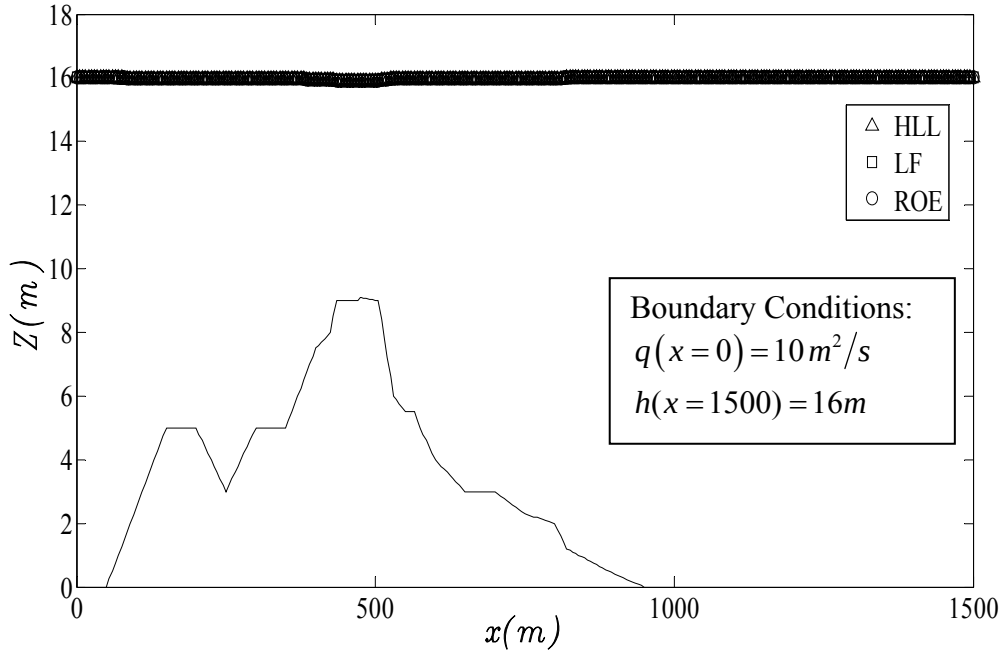

Figure 4-27. Numerical solution of water depth for Test 8 with water surface slope limiter

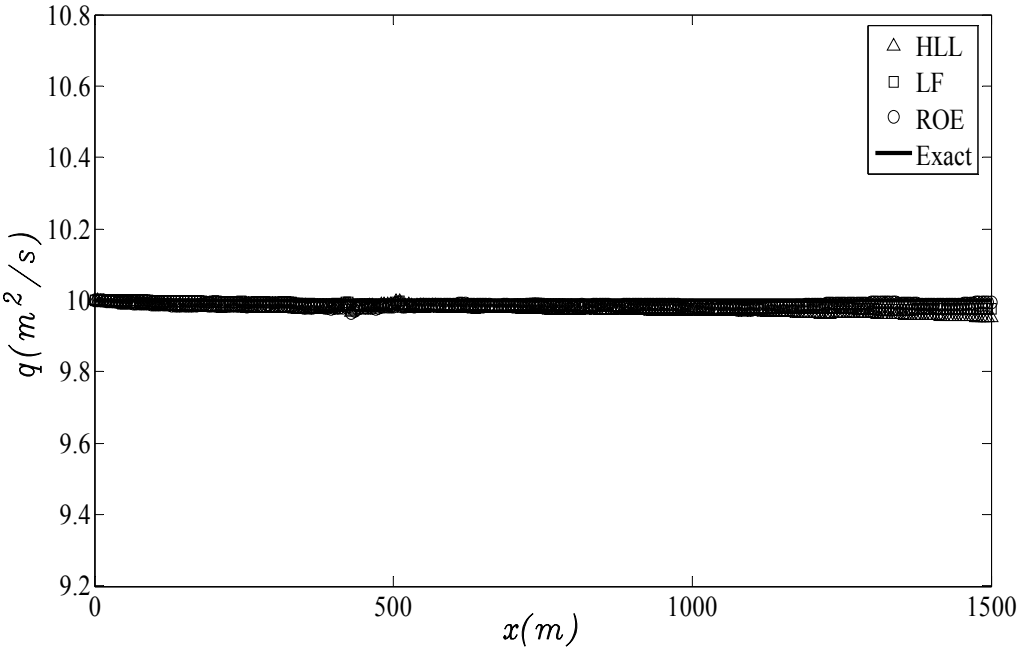

Figure 4-28. Numerical solution of flow rate for Test 8 with water surface slope limiter

Test 9: Transcritical Flow over an Irregular Bed

In this test the irregular bed topography was set as described for Test 7. The flow rate at the inlet was set to be 50 m^2/s and the depth at the downstream end was maintained at 16 m. In this test, the flow regime consists of both subcritical and supercritical flow with a hydraulic jump.

The numerical results are presented in Figure 4-28 to Figure 4-32. The results show that while the water depth is predicted accurately by both slope limiter schemes, the flow rate is predicted more accurately by water surface based slope limiter. In addition, the Roe flux function provides better results for the flow rate when used with either of the two slope limiter schemes.

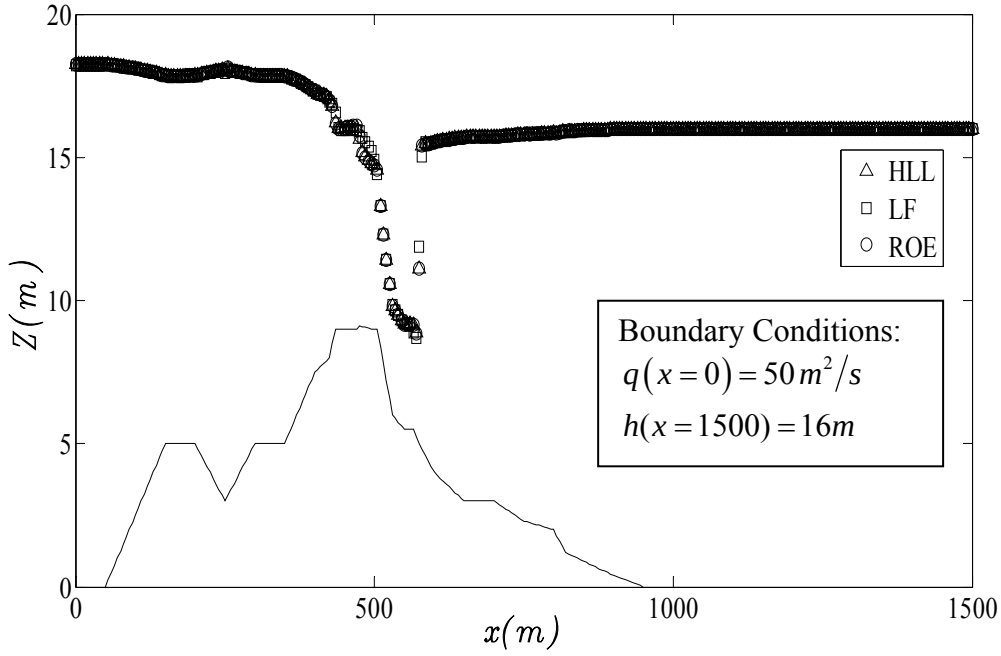

Figure 4-29. Numerical solution of water depth for Test 9 with water depth slope limiter

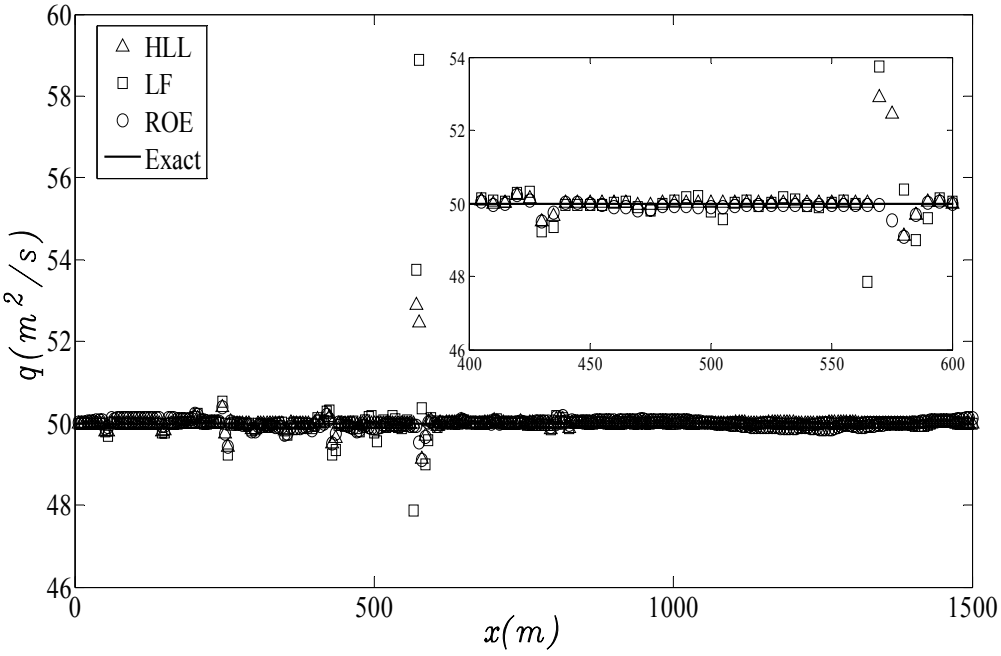

Figure 4-30. Numerical solution of flow rate for Test 9 with water depth slope limiter

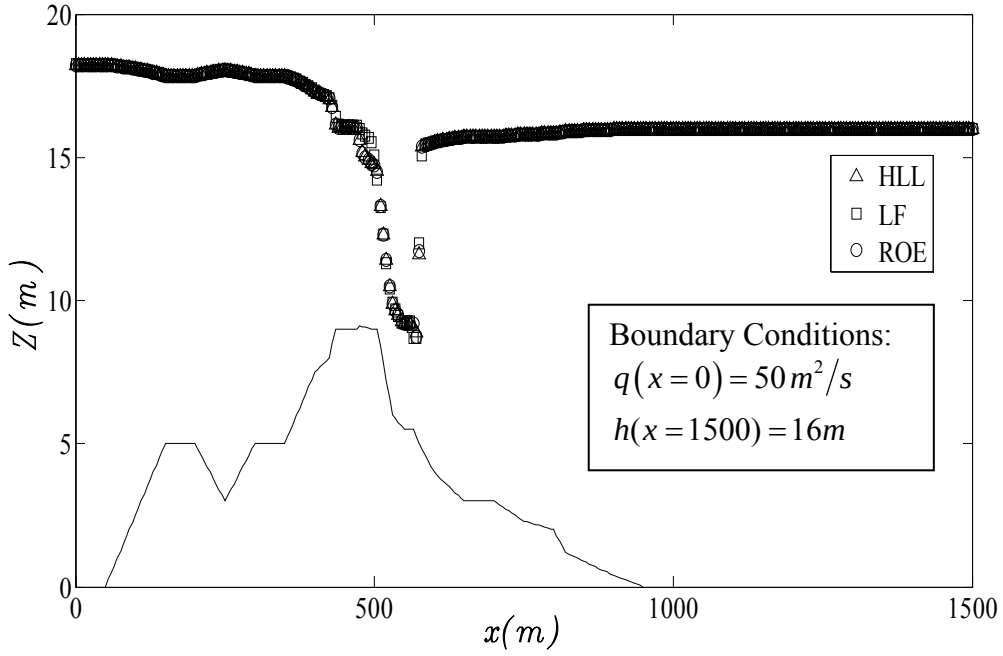

Figure 4-31. Numerical solution of water depth for Test 9 with water surface slope limiter

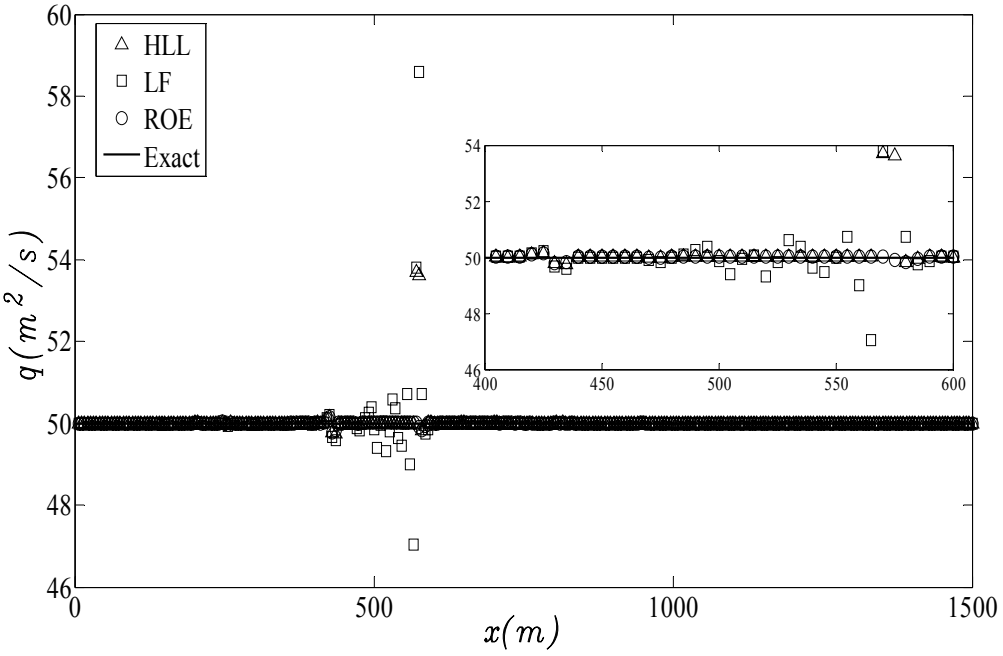

Figure 4-32. Numerical solution of flow rate for Test 9 with water surface slope limiter

CHAPTER FIVE

SUMMARY

A numerical model for one-dimensional shallow water flow is developed using TVD Runge-Kutta Discontinuous Galerkin method with both water surface slope limiter and water depth slope limiter. Numerical tests without source term and with source term due to friction and bed slope are performed. For channels with bed slope variation, numerical tests with both slope limiters are conducted. Different flow conditions including still water, subcritical flow, supercritical flow, and transitional flow regime are investigated.

For each type of slope limiter, Riemann solvers based on HLL, LF, and Roe flux approximation are evaluated. The results prove that water surface slope limiter better preserve the conservative property than the slope limiter based on the water depth. The tests show that Roe flux gives the most accurate results while the LF flux the least accurate.

The slope limiter scheme based on the water depth shows that even for the still water condition (Tests 3 and 7) the zero discharge is not preserved. All three flux functions provide similar results. The results show that the non physical bed slope generated flow increases as the bed becomes more irregular. In the case of water surface based slope limiter, the non physical flow is kept to minimal using all three flux functions. The results show that the water surface based slope limiter preserves the mass conservation property better. In the case of subcritical flow throughout the domain (Tests

4 and 8), the flow depth results based on the two slope limiter schemes follow the same trend as for still water case. However, the results for the flow rate show that overall the LF flux function performs the worst in conserving the flow rate. The Roe flux function has the best overall conservation property. In addition, water depth oscillations are observed with the use of water depth based slope limiter where there is abrupt bed slop change.

In the case where the flow transitions from subcritical to supercritical followed by a hydraulic jump, as in Tests 5 and 9, both slope limiter schemes provide similar results. However, oscillatory results are observed for the flow rate with LF flux function. For both slope limiter schemes, the Roe flux formulation conserves the flow rate most accurately. However, the use of water surface slope limiter with Roe flux provides the best solution. In the case of supercritical flow throughout the domain (Test 6), LF flux function is unable to conserve the initial flow rate.

In general, the water surface based slope limiter is better suited for open channel flows with irregular bed. The tests performed show that the Roe flux function has the best conservation property among the evaluated flux functions.

References:

Aizinger, V., and Dawson, C. (2002). "A discontinuous Galerkin method for two-dimensional flow and transport in shallow water." Adv. in Water Resources, 25(1), 67-84.

Arbogast, T., and Wheeler, M. F. (1995). "A characteristics-mixed finite element method for advection-dominated transport problems." SIAM Journal on Numerical Analysis, 32(2), 404-424.

Catella, A., and Petrere Jr, M. (2008). "Feeding patterns in a fish community of Baia da Onca, a floodplain lake of the Aquidauana River, Pantanal, Brazil." Fish.Manage.Ecol., 3(3), 229-237.

CockBurn B. (2001). "Discontinuous Galerkin Methods for Convection Dominated problems." NATO Lecture Notes.School of Mathhematics, University of Minnesota.

Cockburn, B., Lin, S. Y., and Shu, C. W. (1989). "TVB Runge-Kutta local projection discontinuous Galerkin finite element method for conservation laws III: one dimensional systems." J.Comput.Phys, 84(1), 90-113.

Cockburn, B., and Shu, C. W. (1989). "TVB Runge-Kutta local projection discontinuous Galerkin finite element method for conservation laws II: general framework." Mathematics of Computation, 52(186), 411-435.

Dawson, C., and Aizinger, V. (2005). "A discontinuous Galerkin method for three-dimensional shallow water equations." J.Sci.Comput., 22(1), 245-267.

Einfeldt, B. (1988). "On Godunov-type methods for gas dynamics." SIAM Journal on Numerical Analysis, 25(2), 294-318.

Fraccarollo, L., and Toro, E. F. (1995). "Experimental and numerical assessment of the shallow water model for two-dimensional dam-break type problems." Journal of Hydraulic Research, 33(6), 843-864.

Garcia-Navarro, P., and Vázquez-Cendón, M. (2000). "On numerical treatment of the source terms in the shallow water equations." Comput.Fluids, 29(8), 951-979.

Gharangik, A.M., Chaudhry,M.H. (1991). "Numerical simulation of hydraulic jump." J.Hydraul.Eng., 117 1195.

Gottlieb, S., and Shu, C. W. (1998). "Total variation diminishing Runge-Kutta schemes." Mathematics of Computation, 67(221), 73-85.

Goutal, N., and Maurel, F. (1997). Proceedings of the 2 Nd Workshop on Dam-Break Wave Simulation.

Harten, A., Engquist, B., Osher, S., and Chakravarthy, S. R. (1987). "Uniformly high order accurate essentially non-oscillatory schemes, III." Journal of Computational Physics, 71(2), 231-303.

Harten, A., Lax, P. D., and Van Leer, B. (1983). "On upstream differencing and Godunov-type schemes for hyperbolic conservation laws." SIAM Rev, 25(1), 35-61.

Hughes, T. J. R., Liu, W. K., and Brooks, A. (1979). "Finite element analysis of incompressible viscous flows by the penalty function formulation." Journal of Computational Physics, 30(1), 1-60.

Kubatko, E. J., Westerink, J. J., and Dawson, C. (2006). "hp discontinuous Galerkin methods for advection dominated problems in shallow water flow." Comput.Methods Appl.Mech.Eng., 196(1-3), 437-451.

Li, B. Q. (2006). Discontinuous finite elements in fluid dynamics and heat transfer. Springer Verlag.

Lin, G. F., Lai, J. S., and Guo, W. D. (2003). "Finite-volume component-wise TVD schemes for 2D shallow water equations." Adv.Water Resour., 26(8), 861-873.

Liu, X. D., Osher, S., and Chan, T. (1994). "Weighted essentially non-oscillatory schemes." Journal of Computational Physics, 115(1), 200-212.

Nujić, M. (1995). "Efficient implementation of non-oscillatory schemes for the computation of free-surface flows." Journal of Hydraulic Research, 33(1), 101-111.

Osher, S., and Solomon, F. (1982). "Upwind difference schemes for hyperbolic systems of conservation laws." Mathematics of Computation, 38(158), 339-374.

Perthame, B., and Simeoni, C. (2001). "A kinetic scheme for the Saint-Venant system¶ with a source term." Calcolo, 38(4), 201-231.

Qiu, J., and Shu, C. W. (2005). "Runge-Kutta discontinuous Galerkin method using WENO limiters." SIAM Journal on Scientific Computing, 26(3), 907-929.

Reed, W. H., and Hill, T. (1973). "TRIANGULARMESH METHODSFOR THE NEUTRONTRANSPORTEQUATION." Los Alamos Report LA-UR-73-479.

Roe, P. (1981). "Approximate Riemann solvers, parameter vectors, and difference schemes." Journal of Computational Physics, 43(2), 357-372.

Schwanenberg, D., and Harms, M. (2004). "Discontinuous Galerkin finite-element method for transcritical two-dimensional shallow water flows." J.Hydraul.Eng., 130 412.

Schwanenberg, D., and Köngeter, J. (2000). "A discontinuous Galerkin method for the shallow water equations with source terms." .

Tassi, P., Bokhove, O., and Vionnet, C. (2007). "Space discontinuous Galerkin method for shallow water flows—kinetic and HLLC flux, and potential vorticity generation." Adv.Water Resour., 30(4), 998-1015.

Toro, E. (1989). "A weighted average flux method for hyperbolic conservation laws." Proceedings of the Royal Society of London.Series A, Mathematical and Physical Sciences, 423(1865), 401-418.

Toro, E., Spruce, M., and Speares, W. (1994). "Restoration of the contact surface in the HLL-Riemann solver." Shock Waves, 4(1), 25-34.

Wang, J. S., Ni, H. G., and He, Y. S. (2000). "Finite-difference TVD scheme for computation of dam-break problems." J.Hydraul.Eng., 126(4), 253-262.

Ying, X., Khan, A. A., and Wang, S. S. Y. (2004). "Upwind conservative scheme for the Saint Venant equations." J.Hydraul.Eng., 130 977.

Zhou, J. G., Causon, D. M., Mingham, C. G., and Ingram, D. M. (2001). "The surface gradient method for the treatment of source terms in the shallow-water equations." Journal of Computational Physics, 168(1), 1-25.

Zienkiewicz, O., and Ortiz, P. (1995). "A split-characteristic based finite element model for the shallow water equations." Int.J.Numer.Methods Fluids, 20(8-9), 1061-1080.